

Article

Quantitative Assessment of Strengthening Strategies and Design Recommendations for the Repair of Corrosion-Damaged Reinforced Concrete Members

Udhayasuriyan Brindha ¹, Jeyaprakash Maheswaran ^{2,*}, Maheswaran Chellapandian ¹ 
and Nakarajan Arunachalam ¹ 

¹ Department of Civil Engineering, Mepco Schlenk Engineering College, Mepco Nagar, Sivakasi 626005, TN, India; ubrindha1412@gmail.com (U.B.); chellapandian@mepcoeng.ac.in (M.C.); arunachalam.n@mepcoeng.ac.in (N.A.)

² Department of Civil Engineering, St Xavier's Catholic College of Engineering, Nagercoil 629003, TN, India

* Correspondence: drjmaheswaran@gmail.com

Abstract: Maintenance of reinforced concrete (RC) structures has become a global issue due to the problems associated with the corrosion of steel reinforcement. Corrosion of RC structures results in severe serviceability and strength issues, which in turn necessitates major repair works. Though it is difficult to eliminate the risk of corrosion in RC structures, appropriate retrofitting procedures can be implemented to restore the lost strength. This paper presents a detailed analysis of the mechanism of corrosion in RC members and the procedure for retrofitting corrosion-damaged RC members subjected to different loading conditions. Moreover, the efficiency of existing strengthening techniques, such as steel jacketing, fiber-reinforced polymer (FRP) composites, engineered cementitious composites (ECCs), ferrocement jacketing, fabric-reinforced cementitious composites (FRCMs) and ultra-high-toughness cementitious composites (UHTCCs), are evaluated and compared in relation to restoring/enhancing the performance of corrosion-damaged RC members under different loading scenarios. Moreover, the paper provides a detailed comparison of the effects of different parameters governing the corrosion mechanism and suggests suitable design recommendations for improving the overall performance of corrosion-damaged RC members.

Keywords: corrosion mechanism; design recommendations; damage analysis; retrofitting; repair methods



Citation: Brindha, U.; Maheswaran, J.; Chellapandian, M.; Arunachalam, N. Quantitative Assessment of Strengthening Strategies and Design Recommendations for the Repair of Corrosion-Damaged Reinforced Concrete Members. *Buildings* **2023**, *13*, 1080. <https://doi.org/10.3390/buildings13041080>

Academic Editor: Binsheng (Ben) Zhang

Received: 19 March 2023

Revised: 11 April 2023

Accepted: 16 April 2023

Published: 19 April 2023



Copyright: © 2023 by the authors. Licensee MDPI, Basel, Switzerland. This article is an open access article distributed under the terms and conditions of the Creative Commons Attribution (CC BY) license (<https://creativecommons.org/licenses/by/4.0/>).

1. Introduction

Corrosion is an inevitable process in the construction sector, where it affects the longevity of structural elements and leads to significantly higher costs. Angst [1] highlighted the economic impact of the metallic corrosion of structures in countries such as the USA, India, etc., where it directly affects the gross domestic product (GDP) rate by 3.1%. In 2011–2012, India spent about USD 26.1 billion on the repair and rehabilitation of corrosion-damaged structures [2]. In the United States of America (USA), 15% of the country's total bridge structures experience structural deficiency due to corrosion of steel reinforcement. This implies that 3% (USD 276 billion) of the country's total economy is spent on improving the service life of structures affected by corrosion [3]. It is imperative to comprehend and identify the causes of the failure of structures due to corrosion [4]. Corrosion of reinforced concrete (RC) structures is caused by a multitude of factors, which include (i) age, (ii) carbonation, (iii) inadequate concrete cover, (iv) chloride or salt attack, (v) poor construction quality and (vi) other environmental conditions. Due to these factors, concrete structures absorb oxides and hydroxides from the atmosphere. Moreover, they react with the water present in the concrete, resulting in the formation of corrosion products. This, in turn, lowers the pH value of the concrete below 13 and results in the depletion of the passive layer of the steel reinforcement. Lowering of pH below 11 results in the following

issues: (i) rust development, (ii) development of internal expansive pressure and (iii) brittleness due to reduced sectional area. Hence, the need of the day is to strengthen existing corrosion-damaged structural elements to ensure structural safety and serviceability.

In the construction sector, a number of strengthening methods are deployed for the retrofitting of corrosion-damaged RC structures. The existing strengthening techniques, such as steel jacketing, fiber-reinforced polymer (FRP) composites, ferrocement jacketing, the patch repair technique, fabric-reinforced cementitious composites (FRCMs), engineered cementitious composites (ECCs), mechanically fastened composite systems and the impressed current cathode protection (ICCP) technique, were used for improving the performance of corrosion-damaged RC members. Steel jacketing is a conventional technique used for improving the strength and ductility performance of defective structural elements. Several previous studies have used it for the strengthening of damaged concrete members [5–10]. However, the high initial cost and huge labor and machinery requirements during installation make it one of the least commonly used techniques practically. In recent years, the majority of researchers have focused on deploying advanced composite materials, such as fiber reinforced polymers (FRPs), to restore the capacity of corrosion-damaged RC structures. Different types of fibers, such as carbon, glass, basalt and aramid, are commonly used in the form of wraps or laminates for structural strengthening [11–15]. The matrices or polymers used are mostly of the thermosetting type; i.e., epoxy resin [16–18]. The mechanical properties of FRPs depend on the type of fiber/resin matrix used, the orientation of the fibers, the fiber volume fraction, etc. [19–25]. FRP composites have been successfully used for the repair and strengthening of defective reinforced concrete and prestressed concrete members [26–31]. Despite several advantages, the widespread practical application of FRP composites is hindered due to their high production cost [32]. Moreover, they possess poor thermal stability, which limits their applications in the strengthening of structures exposed to elevated temperatures [33–35]. Due to the drawbacks of FRP composites, several recent research studies have proposed the use of cementitious composites as a replacement for conventional epoxy-based mortar [36–46]. A few of the successful cementitious composites developed and used frequently include (a) fabric-reinforced cementitious matrix (FRCM) composites, (b) engineered cementitious composites (ECCs), (c) ferrocement, etc.

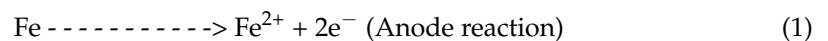
Fabric-reinforced cementitious matrix (FRCM) composites are one of the promising strengthening techniques used in various retrofitting projects for reinforced concrete and masonry structures under different loading combinations [47]. FRCM composites are prepared using a combination of fiber mats and cement-based matrixes. Fibers used as reinforcements in FRCMs include steel, glass, carbon and polyparaphenylene benzobisoxazole (PBO). It is worth noting that the performance of FRCM is mostly dependent on the level of mortar mix penetration, the mechanical properties of the textile used and the spacing of the rovings' used [47]. Similar to the use of FRCM, ECCs, which are also called bendable concrete, have recently been used for structural retrofitting due to their excellent ductile properties, in addition to their strength under both compression and tension [48–51]. These excellent mechanical properties are possible due to the presence of large volumes of discrete fibers. ECCs are an environmentally sustainable building material that utilize more than 50% fly ash as a replacement for cement. Maheswaran et al. [52] concluded that hybrid fiber-based ECCs showed better ductility performance, which helps in keeping the failure plane from moving apart, thereby reducing the brittleness of the members under shear loading. George et al. [53] concluded that the use of ECCs resulted in a large tension strain level of 7%, while conventional concrete has a failure strain of only 0.01% under tension. Ferrocement is also used for strengthening of structures located in marine environmental areas that are highly prone to corrosion [54]. Ferrocement consists of fine steel mesh used as a reinforcing material covered by cementitious matrix [55]. Ferrocement strengthening of deficit RC members can be used to restore their lost strength, stiffness and ductility [56]. In addition to the above strengthening techniques, other methods, such as the patch repair technique using epoxy or an anchorage system, steel fiber-reinforced concrete (SFRC) UHTCCs, mechanically fastened systems and the ICCP repairing technique, have also been

adopted for corrosion-strengthening members [57–70]. However, studies analyzing their effectiveness are not available in large numbers and the issue requires further detailed investigation. The focus of the present work was on providing an in-depth understanding of the corrosion mechanisms of reinforced concrete members resulting from different corrosion-inducing techniques and the procedures for strengthening corrosion-damaged RC members subjected to static and dynamic loads. Moreover, this study provides an extensive discussion on the effects of different design parameters, such as mass loss and strength loss, resulting from different corrosion-inducing techniques and the strength enhancements achieved from various strengthening methods.

2. Corrosion Mechanism and Damage in RC Members

In general, concrete is alkaline in nature, with a pH value of 13 or more. According to Hu et al. [71], the pH is the predominant factor determining whether steel is in a passive or corrosive state. Corrosion of steel reinforcement arises from the reaction between two dissimilar materials in contact with the surrounding environment (such as O₂, CO₂, etc.), resulting in the formation of oxides and hydroxides. In addition, the electrochemical potential seems to be another factor that significantly influences the formation of various chemical substances in a metal. This reaction mechanism destroys the passive iron oxide layer in the reinforcement and tends to decrease the pH value to below 11. This process results in several issues, such as degradation of the bond between steel and concrete, brittle failure and spalling. Though the mechanism of corrosion in RC structures is well-studied, the concept is briefly discussed in the following section to enable the readers to better understand the context.

Figure 1 depicts the Pourbaix diagram, which can be used to understand the concepts of immunity and passivation in relation to concrete reinforcement [72,73]. The Pourbaix diagram, derived from the Nernst equation, is a plot of the equilibrium potential of electrochemical reactions (P) and the pH value. According to the Pourbaix diagram, the electric potential is split-up into three different zones; namely, (a) corrosion, (b) passivation and (c) immunity zones. This classification is mainly based on the thermodynamic data for pure metals. It also consists of two dotted lines (A and B) representing water electrolysis regions. Here, the dotted line A represents the hydrogen line and the dotted line B represents the oxygen line. The zone below the line B is where water evolves to hydrogen gas and hydroxide and the zone above the line B illustrate the evolutions of oxygen and protons. As shown in the figure, both Fe₂O₃ and Fe₃O₄ are stable within the range where the passive film can maintain integrity and resist corrosion. Fe₃O₄ has a high conductivity due to electron hopping between Fe²⁺ and Fe³⁺ ions. Hence, corrosion can be prevented by changing the pH and potential of the electrochemical reactions in the immunity and passivation zones. The iron (Fe) lets out the electrons at the anode and turns into a ferrous state, as shown in Equation (1). The electrons are transferred to the cathode, where oxygen reduction takes place, as shown in Equation (2)



The corrosion of rebar occurs mainly due to two causes, which are discussed below: (a) carbonation-induced corrosion and (b) chloride ion-induced corrosion.

2.1. Carbonation-Induced Corrosion

Carbon dioxide (CO₂) is the primary contributor to corrosion of reinforcement in concrete structures located in urban regions. Moreover, the outdoor air temperature and humidity are two major factors, leading the CO₂ to diffuse into concrete pores and making corrosion occur at a faster rate (10⁴ times faster) in air than in water [74]. Furthermore, CO₂ chemically reacts with the Ca(OH)₂ “portlandite” compound present in the cement

matrix and results in the formation of “calcite” (CaCO₃). This results in the lowering of pH from 13 to 9, thereby making the medium acidic. This acidification, in turn, degrades the passive layer of steel and initiates the corrosion mechanism in steel reinforcement. As a result, uniform corrosion occurs in reinforced steel, as shown in Figure 2, and the reaction is given in Equation (3). Though the effect of carbon-induced corrosion cannot be prevented, its initiation can be delayed by improving the properties of concrete; i.e., use of Portland pozzolana cement, reduction in w/c ratio, etc.

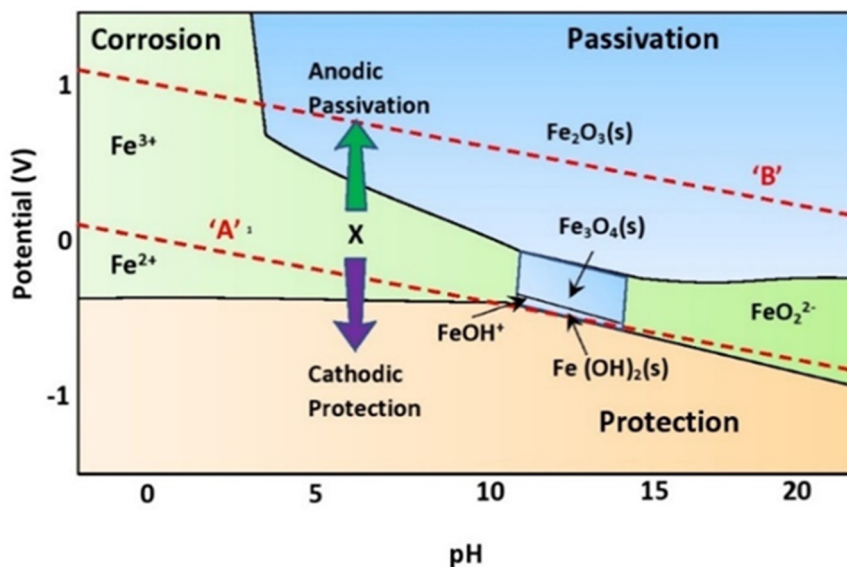


Figure 1. Pourbaix diagram for metals.

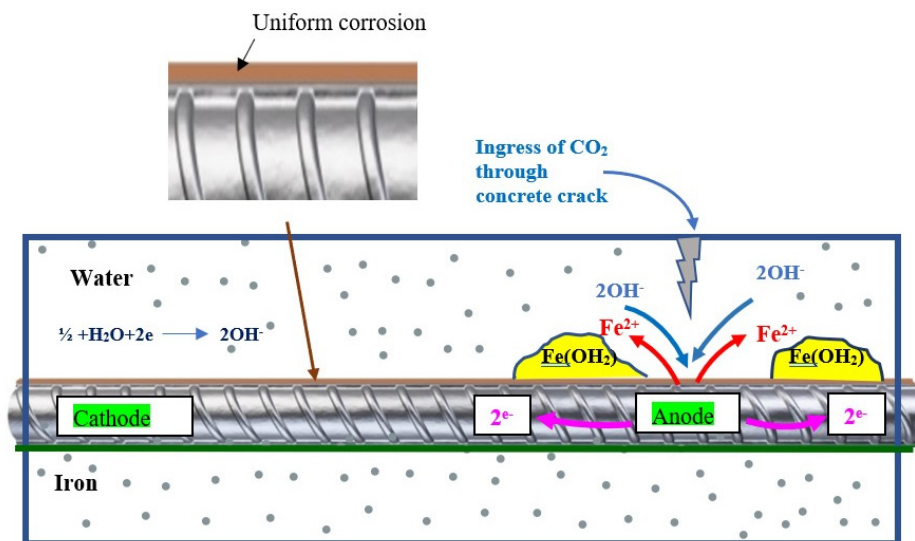


Figure 2. Mechanism of carbonation-induced corrosion.

2.2. Chloride-Induced Corrosion

For RC structures located in extreme marine environments, the occurrence of chloride-induced corrosion is much more common. Chloride-induced corrosion occurs due to the presence of salt contents, such as calcium chloride, magnesium chloride and sodium chloride, in the sea water. These chloride ions penetrate through the pores of concrete and react with the steel reinforcement to form FeCl₂. This FeCl₂ reacts with water to form hydrochloric acid (HCl), which in turn destroys the protective film encompassing

the reinforcement. After de-passivation, stable pitting growth/re-passivation occurs if the $[Cl^- / OH^-]$ ratio falls below a predetermined pH level. When this $[Cl^- / OH^-]$ threshold is exceeded, pitting corrosion occurs and leads to deterioration of the mechanical performance of the member [75]. The schematic representation of chloride-induced corrosion is shown in Figure 3, and its reaction process is shown in Equations (4) and (5).

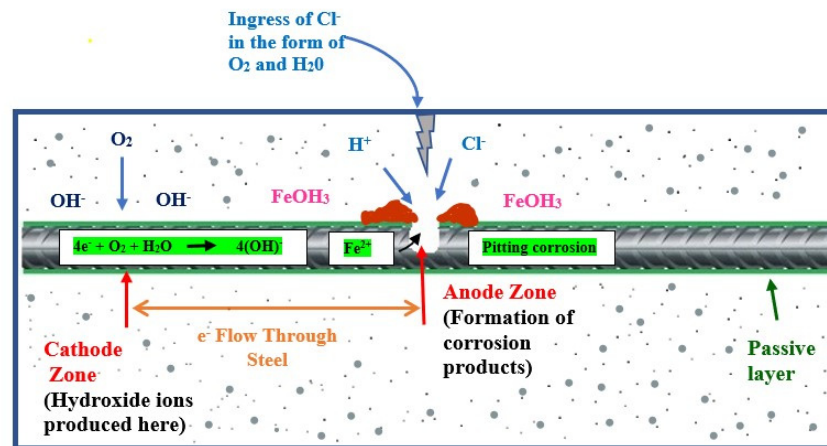
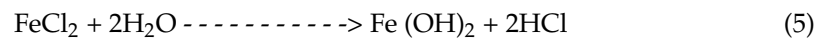


Figure 3. Mechanism of chloride-induced corrosion.

Figure 4 illustrates a schematic depiction of the service life of structures subjected to chlorides. In general, the service life of concrete is mainly dependent on its durability characteristics [76]. The service life is estimated by considering two phases: crack initiation and the propagation phase [77,78]. The initial phase, which is also called the corrosion-free phase, is longer than the propagation phase. However, if the quality of the concrete is poor, the duration of the initial phase will be reduced to a significant extent [78]. The propagation phase is the other phase, which starts once the steel has lost its passivation. In the context of corrosion initiation, determination of the value of the critical chloride threshold is essential. The critical chloride threshold (Cl_{th}) refers to the amount of chloride required to initiate corrosion. However, the estimation of the critical chloride threshold (Cl_{th}) value is challenging as it depends on a number of factors, such as (a) the properties of the concrete cover, (b) the properties of the reinforcing steel and (c) the nature of the steel–concrete interface [79–81]. Rengaraju and Pillai [77] developed an accelerated chloride threshold test with uncoated steel to assess the chloride threshold (Cl_{th}) and to estimate the service life of structures. They evaluated the performances of three different cementitious mortars prepared using ordinary Portland cement (OPC), Portland cement with 30% class-F fly-ash (PPC) and lime-calcinated clay (LC^3) cement. They concluded that the critical chloride threshold value is not an indicator of the service life of structures and the value of Cl_{th} can be improved with the use of pozzolanic material and LC^3 cements. Moreover, they highlighted that the value of Cl_{th} in steel reinforcement is a function of the surrounding cementitious system.

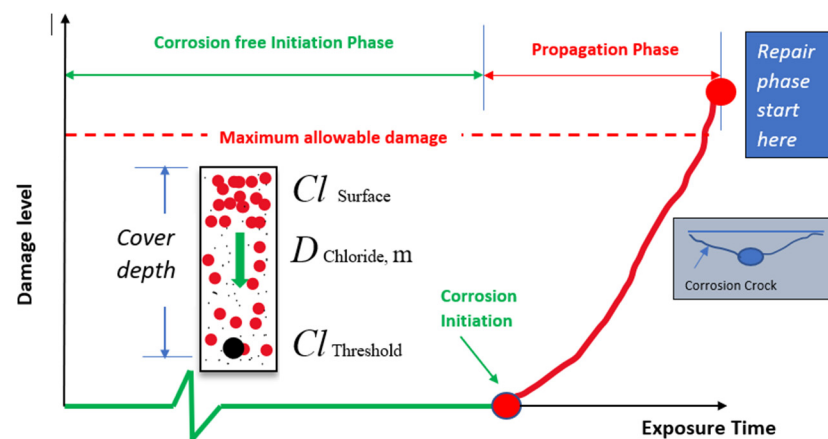


Figure 4. Estimation of service life of concrete in response to chloride-induced corrosion. Note: Cl_{th} —critical chloride threshold; Cl —chloride surface concentration; m —ageing coefficient; and D —diffusion coefficient.

2.3. Impact of Corrosion Process in Natural Environments

In reality, the corrosion mechanism in RC structures is a slow and steady process under natural-environmental conditions (i.e., with the presence of oxygen and moisture). Poupard et al. [82] studied the corrosion interface layer for steel–concrete in a reinforced concrete member subjected to corrosion for a period of 60 years in a natural environment.

The interface layer between steel and concrete observed using an electron microscope is shown in Figure 5. From the observations obtained through the micro-structural analysis, the samples were characterized into two major types: low-level corrosion and high-level corrosion. In the case of the low-level corrosion sample, corrosion took place at 1–4 $\mu\text{m}/\text{year}$ and resulted in the formation/deposition of rust in a uniform fashion throughout the interface. Likewise, the analyses of the high-level corrosion sample showed the development of corrosion at a rate of 8–20 $\mu\text{m}/\text{year}$, and its layer formation was non-uniform, which indicated the occurrence of pitting corrosion (i.e., localized corrosion). In order to ensure structural stability against corrosion, researchers are focusing on the strengthening of corrosion-damaged members at different repair stages. Moreover, to realistically understand the effect of corrosion, researchers have extensively studied the use of advanced techniques, such as artificial corrosion induction. The use of artificial corrosion methods in RC specimens in controlled environments can help to replicate and understand natural corrosion behavior, thereby making it possible to counteract its impact by adopting various strengthening techniques based on the corrosion intensity.

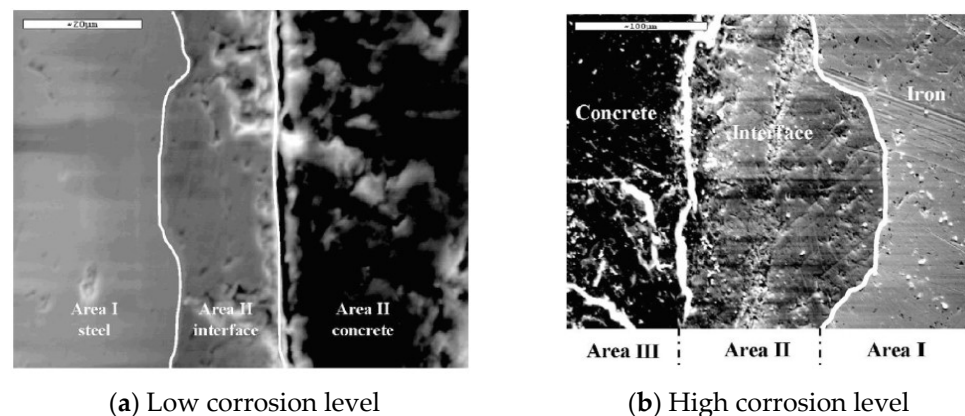


Figure 5. SEM observations at the steel–concrete interface. Reproduced with permission from [82], Elsevier, 2006.

3. Methods of Inducing Corrosion in RC Structures

Several research investigations in the past have studied the mechanism of corrosion in reinforced concrete members using the following techniques: (a) the accelerated corrosion mechanism, (b) artificial climate environments (ACEs), (c) electrochemical chloride extraction (ECE), (d) salt spraying, (e) the potentiostatic accelerated microcell corrosion technique, (f) environmental cycles and (g) freeze–thaw cycles. The effectiveness of different corrosion techniques in helping to understand the real-time behavior of RC members, along with their pros and drawbacks, are discussed in the following section.

3.1. Accelerated Corrosion Process

In general, the process of generating corrosion in RC members in a natural environment takes several years. In order to achieve corrosion in a short period, the accelerated corrosion method is preferred. Figure 6 depicts the electrochemical corrosion process with the accelerated corrosion technique. It is the most widely used method to understand the effect of corrosion on the structural performance of reinforced concrete members. In this method, the corrosion is induced by applying steady power from a direct current (DC) source to steel embedded in concrete that has been dipped in NaCl (saline) solution. The concentration of the NaCl solution is usually fixed in a range based on the time period required to simulate the realistic corrosion effects. Since the corrosion mechanism is an electrochemical reaction, an anode, cathode and electrolytic solution are required. Here, the steel reinforcement embedded in the concrete acts as the anode, an external stainless steel/copper rod acts as the cathode and the aqueous solution of NaCl acts as a medium of ion conduction. In order to witness higher levels of corrosion and the formation of rust, alternate cycles of wetting and drying can be employed to achieve a better oxidation process.



Figure 6. Accelerated corrosion setup. Adapted from [83].

In the work by Jung et al. [83], accelerated corrosion in reinforced concrete was achieved through the modification of parameters such as corrosion duration and current intensity. Kharmia et al. [84] studied an accelerated corrosion process by inducing a low density current at $200 \mu\text{A}/\text{cm}^2$ and spraying 5% NaCl solution over the beam surface for the ingress of chloride penetration. The mass loss of the longitudinal reinforcement was estimated to be 9% and 16.2% at 48 and 96 days, respectively. Moreover, at the

corresponding duration levels, the widths of the developed cracks were measured as 0.8 mm and 1.4 mm, respectively, which were higher than the permissible limits prescribed by the standards. Masoud et al. [85] achieved a mass loss of 9% in RC beams using the impressed current method, and the current density and NaCl solution were fixed at $150 \mu\text{A}/\text{cm}^2$ and 3%, respectively. By evaluating the damaged members, Liu et al. [86] witnessed the occurrence of uniform corrosion along the length of the specimen, which resulted in a reduction in the mechanical strength of the specimen. In addition, transverse cracks parallel to the stirrups and longitudinal cracks with a width up to 1.0 mm up to the level of the bottom reinforcement were also noticed. Nossoni et al. [87] compared the corrosion rates of normal concrete and FRP-wrapped specimens. The normal concrete fused with $11 \text{ kg}/\text{m}^3$ sodium chloride was submerged in a 3% NaCl solution tank. It was subjected to a corrosion process for a period of 130 days, with a constant current of 12 V applied each day every 12 h for a duration of 1 h. The experimental results showed that the mass loss in the unwrapped specimen was higher (20%) compared to the FRP-wrapped specimen.

3.2. ACE and ECE Corrosion Processes

The artificial climate environment (ACE) method employs a climate creation chamber built with corrosion-proof materials [88,89]. This chamber includes a computer-aided operating system for the control of the temperature range, relative humidity and salt or fog flow rate. In this chamber, corrosion is induced in specimens by spraying salt water over the concrete specimen. The flow rate of the salt solution is 150 L/hour. In addition to the above process, an alternate wet–dry cycle process with 5% NaCl solution is also carried out. First, a fog (wet) cycle is employed, which is followed by a drying cycle process with 90% humidity for 4 h. Using the ACE method, studies in the past have concluded that the damage pattern is uniform and includes cracks on the concrete cover and loss in the area of steel of about 2%.

The electrochemical chloride extraction (ECE) method is one of the most extensively used techniques for inducing corrosion in concrete reinforcement [90–95]. This process involves making Fe atoms in the steel reinforcement lose electrons and form oxides through the induction of chloride ions and external energy application [96]. As highlighted in Figure 7, the ECE process is performed by constructing a water tank with a polypropylene resin plate and then coating it with a high-strength cement grout to prevent water leakage. The tank is filled with a 5% NaCl solution with water up to the member's effective height. After that, the electrochemical process is carried out using application of a continuous current. Here, the longitudinal reinforcement acts as a positive pole and the stainless steel immersed in solution acts as a negative pole. It has been found that pitting corrosion occurred on the stirrups and the loss in the area of steel was 7% [96]. This ECE process can also be used to extract chloride ions from concrete to prevent further corrosion in a non-destructive manner.

Dai et al. [96] evaluated two types of corrosion techniques: the artificial climate environment (ACE) method and the electrochemical chloride extraction (ECE) method. The corrosion patterns obtained with the ACE and ECE techniques are compared and presented in Figure 8. From the observations obtained using different corrosion techniques, it can be seen that the use of the ACE technique yielded uniform corrosion over the entire steel reinforcement. The maximum reduction in area obtained with the ACE technique was found to be less than 5%. It is worth noting that this low reduction in area was observed for a period of nearly 6 months, which is comparatively less effective than the other artificial corrosion methods available. In the case of the ECE technique, the corrosion pattern observed was non-uniform; i.e., pitting corrosion at the stirrup location. Moreover, the maximum reduction in the sectional area of the steel stirrups was observed to be 7%, accounting for a corrosion period of nearly 10 days. Hence, comparing the two methods, the use of the ECE technique could produce a non-uniform corrosion pattern in a short

span of time. Moreover, the damage patterns observed were much closer to the real-time observations of corroded structures.

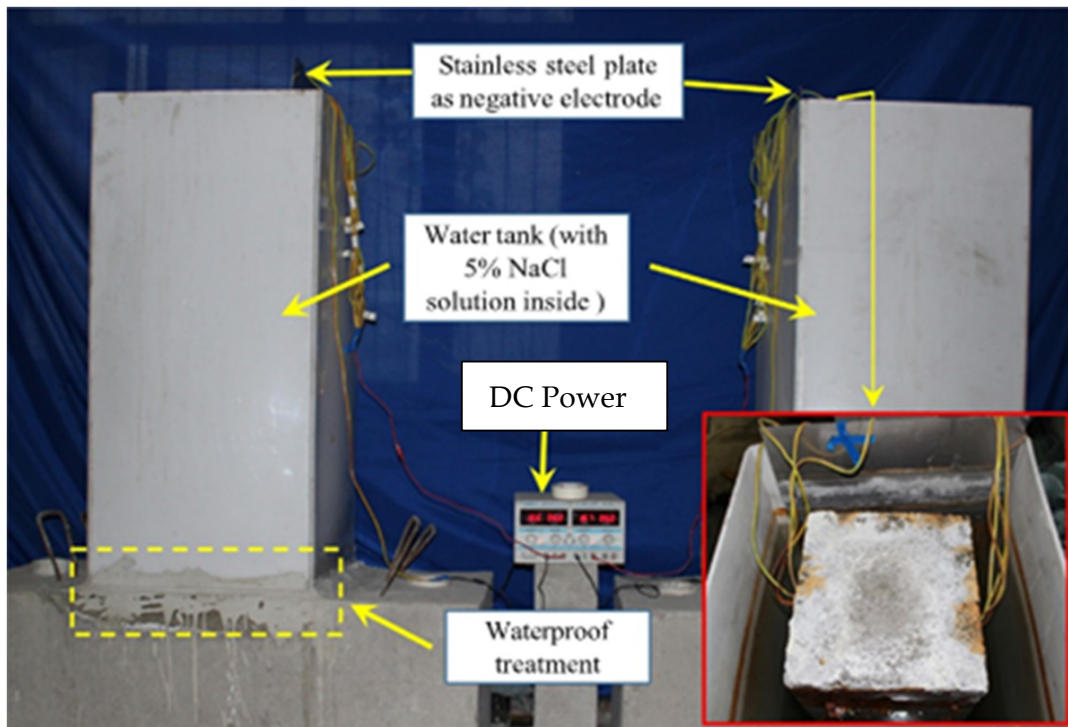
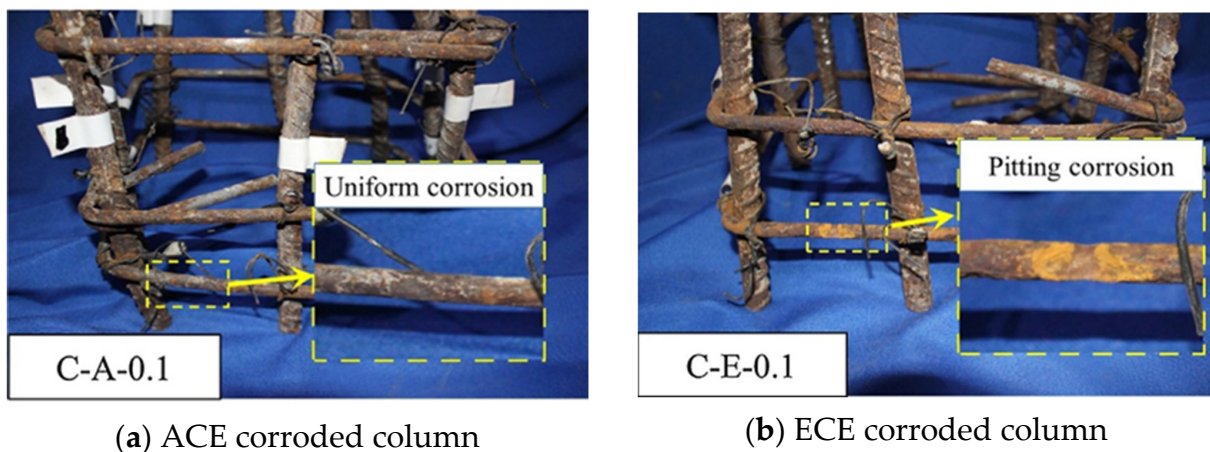


Figure 7. ECE mechanism for inducing corrosion in RC members. Reproduced with permission from [96], Elsevier, 2020.



(a) ACE corroded column

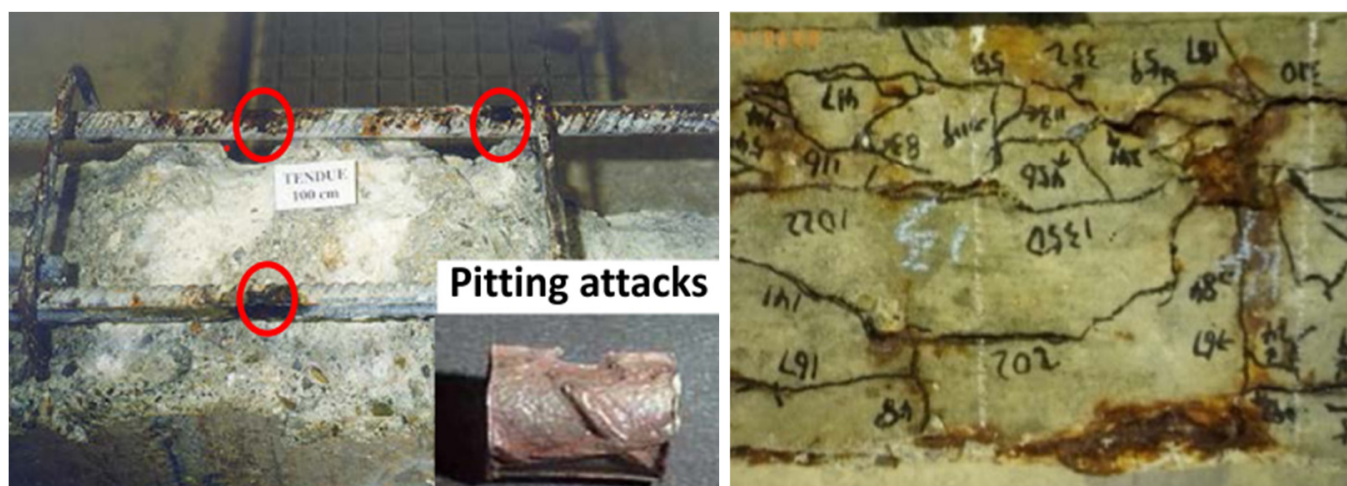
(b) ECE corroded column

Figure 8. Comparison of corrosion patterns with ACE and ECE techniques. Reproduced with permission from [96], Elsevier, 2020.

3.3. Corrosion Initiation by Chloride Spraying

Zhu et al. [97] proposed an alternate method of inducing corrosion in reinforced concrete members. They placed a specimen in a confined room containing four spray nozzles at the corners. A salt fog with an intensity of 35 g/L was sprayed over the specimen continuously for 6 years, after which the continuous spraying was changed to wetting–drying cycles. The corrosion induced after periods of 14, 23, 26 and 28 years in the RC beam was studied. The levels of corrosion at the tension reinforcement were found to be 92.3% and 99.9% at the ages of 26 and 28 years, respectively. This corrosion spread across the entire surface of the steel reinforcement. Moreover, an increase in the degree of corrosion in

the reinforcement above 20% lowered the pitting factor of steel to close to 1. This drastic reduction in pH led to the occurrence of pitting corrosion in the 14th year and rupture of the compression bar and stirrups in the 28th year. Figure 9a highlights the occurrence of pitting corrosion in the compression reinforcement of the beam after 14 years of exposure to the corrosive environment. Figure 9b highlights the longitudinal and transverse cracking at the tension face of the beam. Most of the cracks were spotted along the longitudinal reinforcement (perpendicular to the transverse reinforcement).



(a) Damage after 14 years

(b) Cracking after 28 years in tension zone

Figure 9. Intensities of corrosion damage at different ages in the beam. Reproduced with permission from [97], Elsevier, 2017.

3.4. Potentio-Static Accelerated Macro-Cell Corrosion Technique

Accelerated macro-cell corrosion is generated using a potentio-static macro-cell circuit without drenching the specimen in salt water [98,99]. First, the specimen is wrapped using polyurethane sponges and then re-wetted using a salt solution every 24 h. In addition, AISI type 316 stainless steel mesh can be used to tightly wrap the sponges, acting as a cathode, while the rebar serves as an anode. To reduce the effect of capillary absorption on the initial current readings, the specimens are soaked in water for 24 h prior to the start of the corrosion process. A constant current of 10 V is applied from a DC power supply to initiate the corrosion process. In order to measure the intensity of current, a wireless current data logger can be used to record the corrosion measurements every 10 min.

Fakhri et al. [100] compared the effects of the corrosion rate in cylindrical specimens covered with strain-hardening cementitious composite (SHCC) and conventional concrete specimens by passing chloride ions from salt solution. The corrosion process was allowed to take place for a period of 16 days, achieving a mass loss of 3%. The initial current intensity was measured and found to vary between 52 and 180 μA for the specimens covered with SHCC, while for the conventional concrete-covered specimen, the current intensity varied between 233 and 284 μA . Hence, it was inferred that the use of the SHCC cover as a corrosion protection method resulted in a constant mass loss of 0.057%/h and better electrical resistance due to the fiber bridging mechanism, while the control specimen showed a mass loss of 0.075%/h. The results prove that the SHCC matrix has the ability to limit the corrosion in the initiation phase itself due to its excellent particle-packing capacity and non-conductive nature resulting from the presence of synthetic fibers. Li et al. [101] induced corrosion using the surface coating method in a column saturated with 5% NaCl solution. The column was wrapped with a spongy substance in order to maintain the wetness of the concrete for a period of 3 days. A current of 0.2 $\mu\text{A}/\text{cm}^2$ was applied to the wire connected to the longitudinal reinforcement and the sponge was sprayed with salt fog

every day to maintain its dry–wet conditions. In the test results, the column achieved a mass loss of 20% over a period of 58 days, with a maximum crack width of 0.4 mm. The obtained experimental results were in good concordance with the calculated theoretical mass loss values.

3.5. Freeze–Thaw Cycle Process and Environmental Chambers

The freeze–thaw cycle process can easily deteriorate concrete structures because of the application of alternate cycles of melting and solidification. In extreme humidity conditions, water can penetrate into the pores of concrete through capillary absorption. When the temperature drops, the water freezes and thereby creates hydrostatic pressure, causing the concrete to expand in volume. This results in the formation of numerous micro-cracks in the concrete elements. Due to fluctuations in extreme weather conditions, the frozen water present in the concrete tend to melt completely. Through the repetition of freezing and thawing cycles, numerous gaps are created around the aggregates, thereby resulting in the corrosion of the reinforcement and spalling of the concrete. Several research studies in the past have experimented with the freeze–thaw process to induce corrosion in RC members [102–106]. To maintain the concrete moisture, the RC specimen must be soaked in water for about 4 days before the beginning of the corrosion reaction. Then, the corrosion process is carried out using freeze–thaw machinery, where the temperature is increased and decreased every four hours in the range of $8 \pm 2 \text{ }^\circ\text{C}$ to $-17 \pm 2 \text{ }^\circ\text{C}$ [107]. The specimen should be withdrawn from the machine when the number of cycles required to induce a specific corrosion rate has been reached. In one study, a total of 100 freeze–thaw cycles (23 days approx.) were performed for the RC specimens, which resulted in the formation of macro-cracks.

In another study, an environmental chamber-type corrosion process was carried out by Shang et al. [108]. In this study, the concrete specimen was placed inside the environmental chamber. Similar to the freeze–thaw cycle process specified above, alternate dry–wet cycles were employed in the temperature range between $0 \text{ }^\circ\text{C}$ and $45 \text{ }^\circ\text{C}$. To complete each cycle of the wetting and drying process, the period of 6.2 h was essential. Then, water had to be sprayed over the specimen for three minutes to flush the crystalline salt out from the nozzle. Furthermore, the specimen was fog-sprayed with 5% concentric NaCl solution for three cycles. Each cycle lasted about 20 min and was followed by 40 min without spraying. After that, the temperature was raised from $45 \text{ }^\circ\text{C}$ to $60 \text{ }^\circ\text{C}$ over 30 min at a continuous rate of $0.5 \text{ }^\circ\text{C}/\text{min}$. After the completion of the heating phase, the drying phase was initiated for approximately 2 h. Once the heating phase of 40 min was completed, the temperature was reduced from $60 \text{ }^\circ\text{C}$ to $45 \text{ }^\circ\text{C}$ at a constant rate of $0.37 \text{ }^\circ\text{C}/\text{min}$. This corrosion cycle process must be carried out until the required crack width is attained.

4. Effects of Different Corrosion Techniques and Design Parameters on the Behavior of Reinforced Concrete Specimens

Figure 10 depicts a comparison of the effectiveness of various corrosion-inducing techniques. Among the different methods used, the accelerated current method is easily adoptable and effective in replicating real-time corrosion scenarios in a short period of time. The impressed current technique could yield an average mass loss of 9.5% in steel reinforcement over a shorter time period of 50 days. In the case of the artificial climate environment (ACE) method, the average time period required to induce a mass loss of 2.7% is 167 days. Compared to the impressed current method, the time period required was 70.1% longer and the mass loss achieved was 251.8% lower using the ACE method. In the case of the electrochemical chloride extraction (ECE) method, the time required to induce a mass loss of 7% is very low (i.e., 9 days) when compared to the other techniques. It is worth noting that the time required for the ECE method to induce corrosion effects in RC members is 5 times and 16 times shorter than that for the impressed current and ACE techniques, respectively. Similarly, the use of the potentiostatic accelerated corrosion technique was effective in yielding a mass loss of 3% when subjecting the RC specimen

for a period of 16 days. For the induction of corrosion using the alternate freeze–thaw cycle technique, a high value for the mass loss of up to 12% can be achieved when using a minimum period of 23 days.

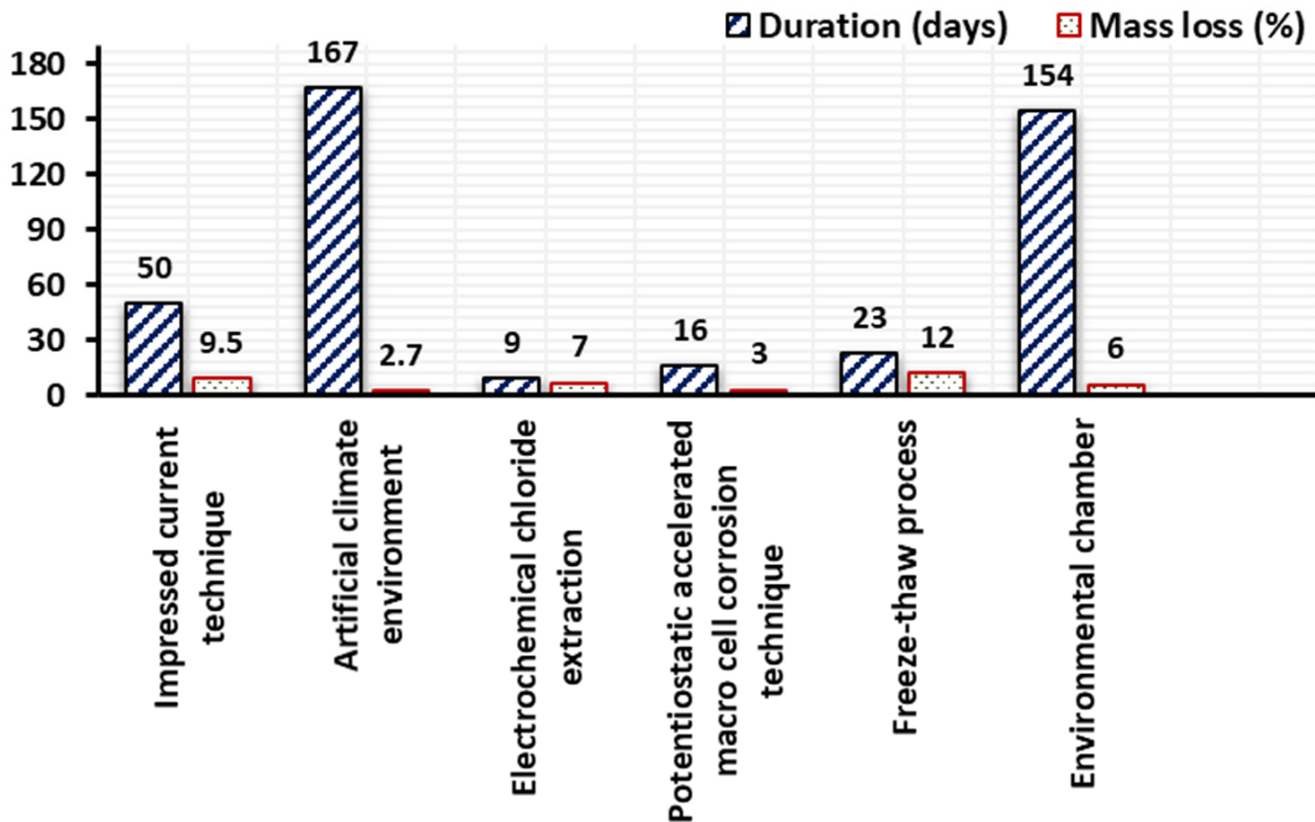


Figure 10. Comparison of different corrosion methods.

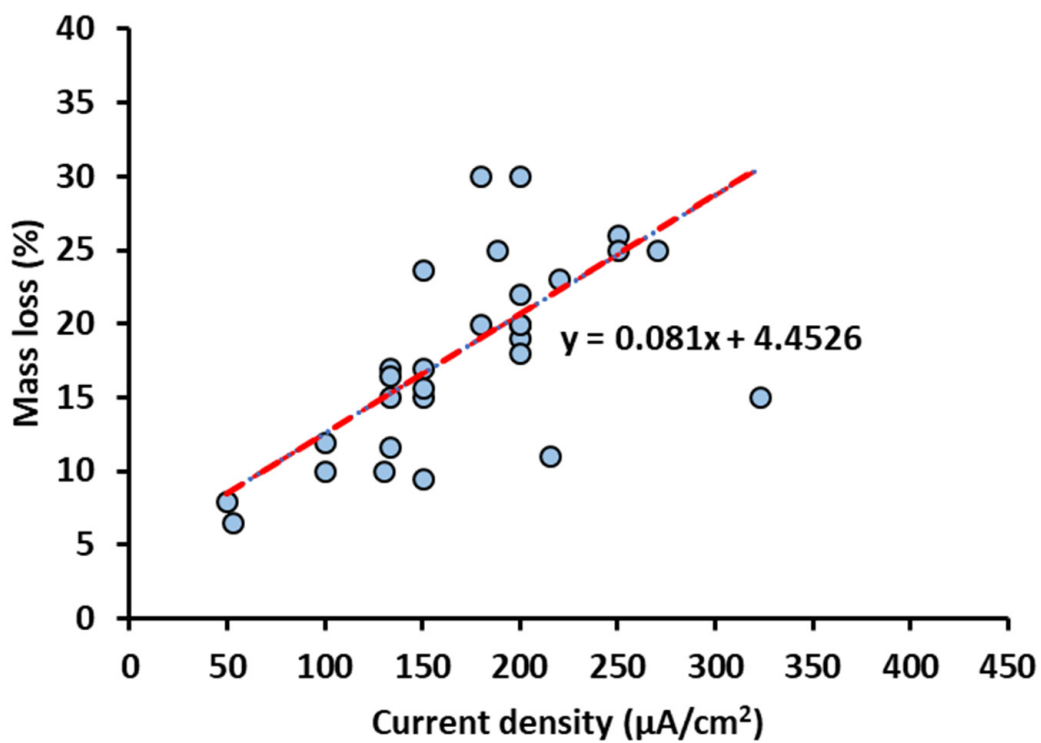
Though the use of the freeze–thaw process to induce accelerated corrosion is highly effective, the practical applicability is hindered by the large initial and running costs. Similar to the ACE method, the use of an artificial environmental chamber yields a low mass loss of 6% with a long exposure period of about five months. To summarize the overall effectiveness of the different methods, it can be noted that techniques such as the artificial climate environment and environmental chamber methods incur high initial and operation costs. Moreover, they also result in lower percentages of mass loss, even though the specimens are subjected for longer time periods. Hence, they are the least preferable techniques for inducing artificial corrosion in RC members. Although a few techniques, such as electrochemical chloride extraction, provide higher mass loss percentages with shorter times, they may result in early shear failure in the specimen [96]. This is because of the introduction of chloride ions and the application of external-energy “Fe” atoms in the steel reinforcement, leading to the loss of electrons, which form oxides, and resulting in a greater reduction in the cross-sectional area of the steel bar. The impressed current technique is a prominent corrosion-inducing method that can produce a reasonable mass loss in an optimal period of time. To bring out the roles of important parameters, such as the intensity of the current applied, the duration required to induce mass loss, etc., several earlier studies were reviewed and the data pertaining to the percentage of mass loss were compared in terms of the current density (data from 33 journal articles) and duration (data from 39 journal articles).

4.1. Design Parameters Affecting the Corrosion of RC Members

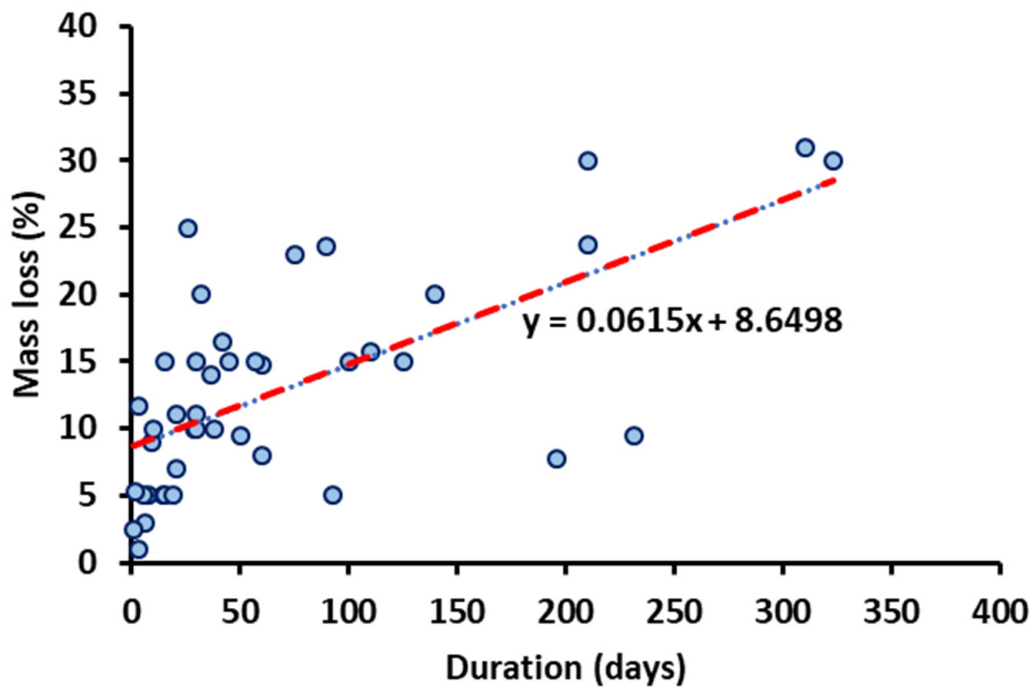
Figure 11 depicts the percentage of mass loss in relation to the duration of the application of current and its intensity. From the literature survey, it was found that the majority of past studies have focused on the use of the impressed current technique to achieve corrosion damage. From the comparisons of the results, it was inferred that the percentage of mass loss is lower in cases of lower current density (up to $60 \mu\text{A}/\text{cm}^2$). However, the mass loss in RC members increases significantly with the increase in the value of the current density. Moreover, with a higher corrosion-inducing time, increased mass loss in the specimen can be observed. A few studies also explained that, with low inducing time and higher current density, a higher mass loss in the specimen can be achieved. Moreover, it was found that most studies observed higher percentages of mass loss (25%) when employing a current density lower than $60 \mu\text{A}/\text{cm}^2$ and an inducing time of less than 60 days.

4.2. Assessment of Previous Equation from Different Design Codes and Studies

The design formulae for the calculation of the current density, penetration rate, corrosion duration, target corrosion ratio and mass loss from various codes and studies are summarized in Table 1. The formulae or equations described in Table 1 are those directly used by researchers in previous studies or improved versions proposed from their studies. The table is only intended to show advancements and recent modifications implemented to predict the actual corrosion ratio in comparison with actual observations from tests. For members subjected to corrosion, it is important to determine the depth of the corrosion penetration rate (CR) and the percentage of mass loss (MR) for the specimens, which can be obtained using Equations (6)–(9), suggested by ASTM-G102-89 [109]. The rate of mass loss in RC members is the ratio of the total anodic current (I_{cor}) applied to the exposure area (A). The values of CR and MR depend on the equivalent weights for pure metals and their atomic weights. Similarly, the value of the current density (I_{cor}) used for inducing specific corrosion levels in RC members is influenced by the depth of the corrosion and mass loss percentage. Zhou et al. [16] estimated the target corrosion ratio (α), which theoretically predicts the mass loss in a specimen. Equations (10)–(12) are used for determining the current intensity and target corrosion ratio (α), which primarily depend on the circumferential area (πdl) of the steel reinforcement. Yang et al. [22] developed an equation (Equation (13)) to calculate the maximum corrosion level (μ_{max}) based on the change in the cross-sectional area of the bar due to corrosion ($A_0(x) - A_{\text{fin}}(x)$), yielding and necking ($\Delta A_{\text{yn}}(x)$) compared to the original cross-sectional area. Zheng et al. [48] estimated the period required for current induction in specimens using Equations (16) and (17). They concluded that the duration of corrosion is proportional to the mass loss in the specimen. As specified in Equation (16), the effect of corrosion duration directly depends on the properties of the materials, such as the radius of steel reinforcement (γ), the densities of the materials (ρ) and the intensity of the current applied. This shows that the duration of corrosion will be longer for specimens reinforced with bars with larger diameters. Moreover, the duration is indirectly proportional to the current intensity (I); i.e., an increase in current density will significantly reduce the total duration required to induce mass loss (%) in the specimen.



(a) Mass loss vs. current density (%)



(b) Mass loss vs. duration (%)

Figure 11. Influences of different parameters on mass loss in steel reinforcement.

Table 1. Theoretical studies used for predicting mass loss and duration.

Reference Study	Formulae Used for Predicting the Corrosion Process
ASTM-G102–89 [109]	a. Calculation of corrosion current density
	$i_{\text{cor}} = \frac{I_{\text{cor}}}{A} \quad (6)$
	b. Calculation of penetration rate (CR) and mass loss rate (MR)
	$\text{CR} = \left(K_1 * i_{\text{cor}} * \frac{\text{EW}}{\rho} \right) \quad (7)$
	$\text{MR} = (K_2 * i_{\text{cor}} * \text{EW}) \quad (8)$
	$\text{EW} = \frac{1}{\frac{\sum n_i f_i}{W_i}} \quad (9)$
Zhou et al. [16]	Calculation of corrosion density
	$i = \frac{1}{n\pi dl} \quad (10)$
	Calculation of target corrosion ratio
	$\alpha = \frac{M_{\text{it}}}{F\alpha\rho} \quad (11)$
	Calculation of actual average corrosion level
	$\mu_{\text{avg}} = \frac{\frac{\mu_{\text{loss}}}{\text{mid length of the rebar}}}{\frac{\mu_{\text{bar}}}{\text{tensile bar length}}} \quad (12)$
Yang et al. [22]	Calculation of maximum corrosion level
	$\mu_{\text{max}} = \frac{\max(A_0(x) - A_{\text{fin}}(x) - \Delta A_{\text{yn}}(x))}{A_0(x)} \quad (13)$
Hou et al. [42]	Calculation of actual corrosion ratio
	$\rho = \frac{\Delta m}{m_0} \quad (14)$
	Calculation of corrosion duration using Faraday's law
	$t = \frac{zF\Delta m_t}{MiS} \quad (15)$
Zheng et al. [48]	Calculation of corrosion duration according to Faraday's law
	$t = \frac{ZF \cdot r \cdot \rho\eta_s}{2M \cdot i} \quad (16)$
	Calculation of mass loss in stirrups
	$\eta = \left(\frac{\frac{m_0}{l_0} - \frac{m_1}{l_1}}{\frac{m_0}{l_0}} \right) \times 100 \quad (17)$
Fakhri et al. [100]	Faraday's law of electrolysis
	$m = \frac{A}{Z \cdot F} \int_0^t i dt \quad (18)$

Table 1. Cont.

Reference Study	Formulae Used for Predicting the Corrosion Process
	Calculation of mass loss using Faraday's law
Joshi et al. [110] Jia et al. [111]	$\Delta m = MI t / zF \quad (19)$
Siad et al. [112] Zhang et al. [113] Daneshvar et al. [114]	Calculation of mass loss ratio for reinforcement bars
	$\rho = \frac{M_1 - M_2}{M_1} \times 100\% \quad (20)$
	Calculation of mass loss using Faraday's law
	$M^{th} = \frac{(W \times I_{app} \times T)}{F} \quad (21)$
	Calculation of actual mass of rust per unit of surface
	$M_{ac} = \frac{W_i - W_f}{\pi \times D \times L} \quad (22)$
Alwash et al. [115]	Calculation of degree of induced corrosion
	$\rho = \frac{W_i - W_f}{W_i} \times 100 \quad (23)$
	Calculation of equivalent current density
	$I_{app.} = I_{corr.} = \frac{\rho \times w_i \times F}{100 \times \pi \times D \times L \times W \times T} \quad (24)$
	Calculation of natural corrosion power
	$NCP = R \times t \times S \quad (25)$
	Calculation of total volume deduction
Wang et al. [116]	$\Delta V = \frac{I \cdot t \cdot M}{n \cdot F \cdot \rho} \quad (26)$
	Calculation of diameter size of corroded bar
	$D_i^C = \sqrt{\left(D_i^0\right)^2 - \frac{\Delta V_i \cdot 4}{\pi \cdot N_i \cdot L_i}} \quad (27)$
	Calculation of corrosion duration using modified Faraday's law
	$t(\text{sec}) = \frac{\alpha \cdot m_{\text{loss}} \cdot n_{\text{specimen}} \cdot C_{\text{Faraday}}}{\text{Current}(A) \cdot M_{\text{specimen}}} \quad (28)$
Rajput et al. [117]	Calculation of λ factor (if the mass loss is less than the theoretical mass loss)
	$\lambda = \frac{\text{Theoretical mass loss}}{\text{Actual mass loss}} \quad (29)$

Table 1. Cont.

Reference Study	Formulae Used for Predicting the Corrosion Process
	Calculation of weight loss using Faraday's law
Pantazopoulou et al. [118]	$\Delta W(g) = \frac{I \cdot t \cdot A_m}{z \cdot F} \quad (30)$
	Calculation of mass loss in reinforcement using mass corrosion rate ρ_w
	$\Delta m = \frac{\pi}{4} d_b^2 L \rho \rho_w \quad (31)$
Shen et al. [119]	Calculation of corrosion initiation
	$t = \frac{\pi d_b^2 L \rho \rho_w z F}{4 M I} \quad (32)$

Fakhri et al. [100] calculated the mass loss in a specimen using the integration technique. As shown in Equation (18), the mass loss value is based on the current intensity and change in time (dt) with the limits ($\int_0^t dt$). Moreover, the percentage of mass loss (%) can be calculated from the changes in mass after corrosion exposure compared to the original mass. Shen et al. [119] calculated the loss in steel reinforcement using Equations (31) and (32). They concluded that the mass loss in steel reinforcement depends on the diameter of the bar (d_b), the length of the bar (L) and the density of the material (ρ). Jia et al. [111] derived an equation for the change in mass loss for a specimen (Δm). As per the equation, the mass loss in the specimen depends mainly on the mass of the specimen (Δm), the current intensity (I) and the duration of the application of current (t). In addition, the corrosion duration (t) can also be calculated using Equation (18), which is similar to the equation proposed by the previous researchers. Alwash et al. [115] developed an equation to identify the degree of corrosion (ρ) based on the difference in the weight of the specimen prior to and after corrosion. Wang et al. [116] estimated the power of natural corrosion (NCP) in steel reinforcement based on the corrosion rate, duration and surface area. The study found that the majority of researchers apply Faraday's I law, which is explicit and simpler to use to estimate the mass loss in reinforcement (Δm) during the accelerated corrosion process. Rajput et al. [117] developed the corrosion factor (λ), which was defined as the ratio of the theoretical mass loss to the actual experimental mass loss.

First, it is essential to understand the accuracy of the theoretical predictions proposed by different researchers, as the process of corrosion is complex and involves multiple factors affecting the results considered. The accuracy of the percentage of mass loss is calculated by comparing the theoretical mass loss values with the actual test results, as shown in Figure 12. In the figure, it can be observed that the majority of researchers calculated the theoretical mass loss rate using Faraday's I and II laws and the actual mass loss rate from gravimetric testing using ASTM-G102-89 [109]. The benchmark of a mass loss rate less than or equal to 20% was adopted by the majority of the researchers in the experiments for studying the corrosion process of reinforcement bars, while only few researchers experimented with specimens with a mass loss in the reinforcement bar greater than 20%. It can be noted that a mass loss rate of less than 30% has been marked as a reference rate for corrosion testing of reinforcement bars. Alwash et al. [115] induced corrosion by applying 700 μA current density for periods of 8 and 32 days. With the accelerated corrosion technique, they obtained actual mass losses of 5.5% and 20.7% at 8 and 32 days, respectively. Moreover, the theoretical mass losses for the same specimen were 5% and 30%, showing minimal deviations between tests and theoretical calculations. Rajput et al. [117] obtained the actual mass loss with application of 200 $\mu A/cm^2$ current and found that the actual mass loss was 30.2%. Similarly, the theoretical mass loss calculated using the modified Faraday's law was found to be 30%. Hence, the results are in concordance with each another, and it can be

suggested that the modified Faraday's law is the most preferable formula for calculating the mass loss rate.

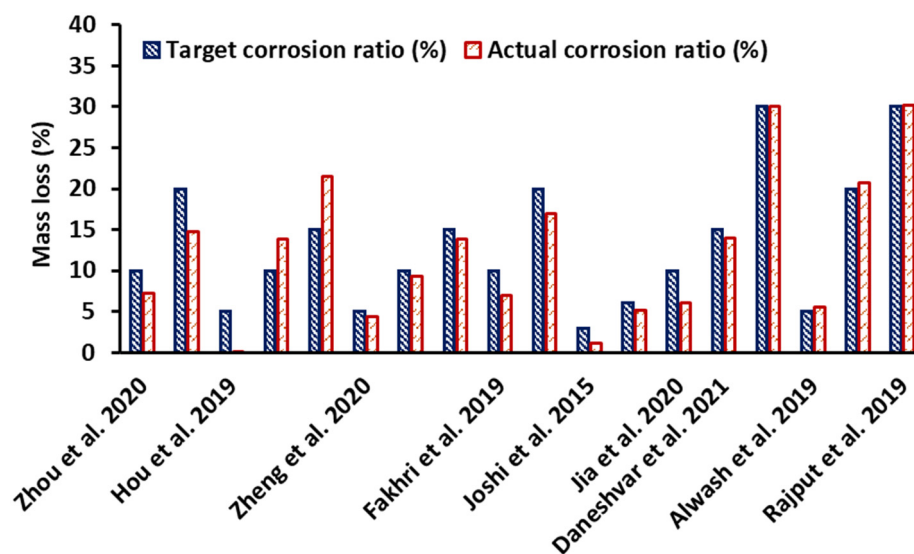


Figure 12. Comparison of the theoretical and actual corrosion ratios [16,42,48,100,110,111,114,115,117].

5. Repair Methods for Corrosion-Damaged Reinforced Concrete Members

Before initiating the process of strengthening, it is essential to remove the surface contaminants from the existing corroded concrete surface to achieve a better bond between the new concrete and substrate. The various types of surface preparation methods used for patch repair of corrosion-damaged members are depicted in Figure 13. In most cases, the wire-brushing method is used in the first instance to remove the corrosion products from the existing steel reinforcement. To remove the dust and loose particles present after the removal of debris, vacuum cleaning and mechanical scrubbing methods are used so that the bond remains intact between the old and new concrete. In certain cases, the sand-blasting method is used to remove the salt-contamination rust products present in the RC members. After careful analysis of the intensity of damage and initial surface preparation, the appropriate strengthening method can be selected. Figure 14 depicts the various retrofitting schemes commonly used for enhancing the performance of corrosion-damaged RC members. First, it is essential to determine whether the severity of the damage is major or minor. In the case of minor damage in the form of surface cracking, where the intensity is lower, it may be sufficient to use corrosion inhibitors (either organic or inorganic). However, if the intensity of damage is severe, in the form of concrete spalling and extensive cracking, then the use of the appropriate strengthening scheme is essential, in addition to the use of corrosion inhibitors and surface preparation methods. Table 2 provides a detailed summary of previous studies on the retrofitting methods used for corroded RC members under different load combinations.

Table 2. Summary of studies on the retrofitting of corroded RC members.

Reference	Specimen and Load Type	Corrosion Type	Repair Method	Intensity of Damage	Enhancement Observed
Kaya et al. [12]	Steel columns under axial compression load	Different patterns of simulated corrosion	Concrete-filled GFRP jacket	Global buckling, delamination of GFRP	Use of two and three layers of GFRP enhanced load-carrying capacity by 9% and 26%
Zhou et al. [16]	Circular RC column under seismic loading	Impressed current method (3.5% NaCl)	LRS-FRP wrap	Several horizontal cracks, larger flexural deformation in the plastic hinge zone	<ol style="list-style-type: none"> 1. The energy dissipation capacity increased by 371.8% and 1040% for 0.2 and 0.4% P_u 2. Shift in failure mode from brittle shear-compression failure to ductile flexure mode
Haddad et al. [17]	RC beam subjected to four-point bending test	Impressed current method (3.0% NaCl)	CFRP sheets at different configurations with CFRP anchors	Concrete and spalling of cover concrete	Increases in load-carrying capacity by 37% and flexural stiffness by 54%
Chotickai et al. [18]	RC column under eccentric compression	Impressed current method (5% NaCl)	CFRP wrapping	Extensive cracking on the tension face and on the compression face	Increase in load-carrying capacity by 20%
Jayaprakash et al. [20]	RC column under axial and eccentric loading	Impressed current method (5% NaCl)	Hybrid combination of CFRP and GFRP strengthening systems	Crushing of concrete, rupture of FRP on tension face and buckling of FRP on the compression face	<ol style="list-style-type: none"> 1. Increase in strength by 8% and 27% for one and two plies of GFRP wrapping 2. Increase in strength by 17% and 33% for one and two plies of CFRP wrapping 3. Increase in strength of 36% for one ply of GFRP and CFRP wrapping
Tigeli et al. [21]	RC beam subjected to four-point bending test	Impressed current method (5% NaCl)	Cementitious patch repair and CFRP laminates	Delamination of CFRP laminates	<ol style="list-style-type: none"> 1. Increase in strength by 25% for patch repair technique and 50% for CFRP technique 2. Increase in stiffness by 5% for patch repair technique
Yang et al. [22]	RC beam subjected to four-point bending test	Salted concrete with 3% NaCl (submerged to mid-span)	Hybrid FRP strengthening + CFRP U-jackets	Rupture of the GFRP laminate and anchorage failure in CFRP jackets	Increase in flexural strength by 57%, 165% and 417% for CFRP U-jackets, GFRP laminates and hybrid strengthening, respectively.

Table 2. Cont.

Reference	Specimen and Load Type	Corrosion Type	Repair Method	Intensity of Damage	Enhancement Observed
Kalyoncuoglu et al. [23]	Substandard RC column under combined axial and lateral cyclic loading	Externally spraying with calcium chloride	Two plies of CFRP wrapping	CFRP rupture and cover concrete spalling	Increase in energy dissipation capacity up to 3% (drift ratio)
Badawi et al. [25]	RC beam subjected to four-point bending test	Salted concrete with 2.25% NaCl and 100% humidity	CFRP wrapping	Rupture of CFRP composites	Increase in flexural yield load by 19% and ultimate capacity by 50%
Li et al. [26]	RC column subjected to monotonic axial compression test	Impressed current method (5% NaCl)	Large rupture strain CFRP strengthening	Buckling of rebar and concrete deterioration in highly corroded specimens	Energy absorption capacity for LRS-FRP was significantly improved when compared with only CFRP strengthening
Karimipour et al. [27]	RC square column under cyclic loading	Salted concrete with 4% NaCl	GFRP and CFRP jacketing	Fabric separation, de-bonding and tearing of FRP fabric	Increase in ductility by 30% and 60% for CFRP and GFRP fabric-strengthened specimens
Do-Dai et al. [30]	RC beam subjected to four-point bending test	Impressed current method (4.5% concentric H ₂ SO ₄)	EB-CFRP laminates, EB-BFRP laminates and CFRP U-wrap anchors	FRP debonding, rupture of CFRP and BFRP	CFRP anchorage system enhanced strength by 87.6%–104.8% and decreased ductility index by 4.5%–28.9%
Liu et al. [36]	Continuous RC beams subjected to fatigue test	Not specified	Polarized carbon FRCM plate under ICCP-SS	Fracture of longitudinal bar, crushing of concrete	Decrease in strength due to degradation of carbon FRCM plate due to polarization
Elghazy et al. [37]	RC Beam subjected to four-point bending test	Impressed current method (5% NaCl)	PBO-FRCM and carbon FRCM strengthening	FRCM delamination, fabric slippage, CFRP laminate rupture, matrix cracking and fabric separation	PBO-FRCM increased ultimate load-carrying capacity and ductility, while C-FRCM showed better post-yielding stiffness
Elghazy et al. [40]	RC beam subjected to four-point bending test	Potential-static technique Salted concrete with 5% salt solution	FRCM composite	Matrix cracking, fiber delamination, concrete crushing, PBO fabric debonding from matrix	Increase in strength by 65%
Elghazy et al. [41]	RC Beam subjected to four-point bending test	Impressed current method (5% NaCl)	FRCM composites (PBO and carbon)	Delamination of PBO-FRCM and concrete crushing	1. Increases in strength for PBO-FRCM and CFRCM by 107–129% and 155%, respectively 2. Increase in fatigue life by 38–377%
Jayasree et al. [44]	RC beams subjected to four-point bending test	Impressed current method (4% NaCl)	Ferrocement with two layers of wire mesh	Crushing and spalling of concrete cover	Increase in ultimate load-carrying capacity for low and medium corrosion rates

Table 2. Cont.

Reference	Specimen and Load Type	Corrosion Type	Repair Method	Intensity of Damage	Enhancement Observed
Hu et al. [50]	RC beam subjected to four-point bending test	Impressed current method (5% NaCl)	Hybrid CFRP-ECC scheme	Micro-cracks in ECC layer and rupture of CFRP wrap	Increases in strength of 28.0%, 24.0% and 19.0% for the corrosion levels of 3.7%, 8.3% and 13.2%
Hou et al. [63]	RC beams subjected to four-point bending test	Post-corrosion	Ultra-high-toughness cementitious composites (UHTCCs)	Splitting cracks near free end, diagonal cracks at beam web	Decrease in bond strength by 12–13.5% for post-corrosion specimens and by 13.5–18% for pre-corrosion specimens
Su et al. [68]	Continuous RC beam subjected to five-point bending test	Impressed current method with two dry–wet cycles per week	Two layers of carbon fiber mesh	Concrete crushing, interfacial separation of CFRP and de-bonding at tension zone	Increase in yield load by 10.5%–52.3% compared to the reference beam
Joshi et al. [110]	Short RC columns under axial loading	Impressed current method (3.5% NaCl)	Ferrocement and GFRP wrapping	Failure of ferrocement jacket, rupture of CFRP sheet	Increase in strength by 77% for 3.51% corrosion level and 59% for 5.9% corrosion level.
Jia et al. [111]	RC bridge column under seismic loads	Impressed current method (3.5% NaCl)	CFRP jacketing	Cover concrete crushing, extensive crack formation	1. CFRP jacketing did not restore the strength but significantly improved the ductility
Siad et al. [112]	RC beam subjected to four-point bending test	Impressed current method (5% NaCl)	CFRP wrapping	Debonding of CFRP layers	Increase in strength when compared to the unstrengthened beam
Zhang et al. [113]	Recycled aggregate concrete beams subjected to four-point bending test	Impressed current method (5% NaCl)	CFRP wrapping	Debonding of CFRP, concrete crushing, diagonal cracks	Corrosion-damaged and strengthened specimen enhanced maximum deflection by 30% compared to strengthened uncorroded specimen
Daneshvar et al. [114]	RC slab under multi-impact loading	Impressed current method (3.5% NaCl)	Externally bonded BFRP	Debonding of CFRP sheets and severe crack formation	Decrease in energy absorption capacity by 77% for 15% corrosion level and 89% for 30% corrosion level
Alwash et al. [115]	RC beams and columns under combined axial and bending loads	Impressed current method (5% NaCl)	Patch repair technique	Extensive concrete crushing and rupture	Increases in ductility by 19% and 42% for low and high corrosion levels, respectively Strength not restored for either corrosion level
Wang et al. [116]	RC beam subjected to four-point bending test	1. Galvanic corrosion accelerated by electric current 2. Natural corrosion	FRP patching repair technique with U-shaped anchorage strips	Concrete crushing without yielding of rebar, debonding of longitudinal FRP strips	Increase in load-carrying capacity by 13%

Table 2. Cont.

Reference	Specimen and Load Type	Corrosion Type	Repair Method	Intensity of Damage	Enhancement Observed
Wang et al. [120]	Prototype RC bridge pier subjected to quasi-static cyclic test	Impressed current method (3.5% NaCl)	UHPC jacketing	Crushing and spalling of UPHC cover	Decreases in stiffness and strength by 3.6% and 3.7%, respectively
Li et al. [121]	RC stub column subjected to axial and cyclic lateral loading	Impressed current method (3.5% NaCl)	Combination of CFRP wraps and steel jacketing	Rupture of steel angle, concrete crushing	Increases in strength by 93.2% and ductility by 122.3%
Yousefi et al. [122]	Circular hollow steel columns under axial compression	Impressed current method (5% NaCl)	CFRP jackets	Rupture of CFRP	Increase in ductility by 2%
Tastani and Pantazopoulou [123]	RC columns under axial compression	Electrochemical corrosion method (5% NaCl)	Carbon and Glass FRP	FRP rupture	Increase in strength and ductility when compared to the original specimen
Triantafyllou et al. [124]	RC beam subjected to four-point bending test	Impressed current method (3.0% NaCl) with wet-dry cycles	NSM and EB FRP strengthening	Debonding and concrete crushing	Maximum load enhancements of 44.4% and 22.1% were observed for NSM- and EB FRP-strengthened beams, respectively.
Ray et al. [125]	RC beams subjected to four-point bending test	Impressed current method (5% NaCl)	CFRP wraps and FRP spike anchor	FRP delamination and FRP rupture	Increases in stiffness by 20% and 11% for PMC-FRP- and CFO-FRP-strengthened specimens
Lee et al. [126]	RC columns under axial compression	Impressed current method (3.5% NaCl)	CFRP confinement	Circumferential expansion around the CFRP wraps	Increase in strength by 50% and decrease in corrosion rate by 50% in post-repair corrosion process
EI-Maaddawy et al. [127]	RC beams subjected to four-point bending test	Mist spraying with fogging compressed air nozzles	CFRP wrapping	Rupture of CFRP composite	Increase in strength by 40% for the fully wrapped CFRP specimen
Sahmaran et al. [128]	Prism with centrally placed deformed bar under four point bending test	Impressed current method (5% NaCl)	Engineered cementitious composites	Microcracks in ECC, concrete spalling, longitudinal cracks.	Decrease in load-carrying capacity by 34% and 45% for the corrosion process of 25 h and 50 h respectively.
EI-Maaddawy et al. [129]	RC beam subjected to four-point bending test	Impressed current method (3.0% NaCl)	FRP composite plates with power-actuated fasteners, expansion and threaded anchor bolts	Rupture of CFRP, concrete crushing and load-bearing failure at plates	1. EAB and TAB enhanced strength by 81%–85% 2. PAF enhanced strength by 67% and decreased ductility index by 33%

Table 2. Cont.

Reference	Specimen and Load Type	Corrosion Type	Repair Method	Intensity of Damage	Enhancement Observed
Radhi et al. [130]	RC column under axial compression	Impressed current method (3.5% NaCl)	CFRP jackets	Rupture of CFRP fabric	1. Increases in strength by 167% and 216% for one and two layers of CFRP wrapping 2. Decreases in strain levels by 23%, 42% and 48% for 10%, 20% and 30% corrosion levels
Al-Akhras et al. [131]	RC columns under eccentric compression	Impressed current method (3% NaCl)	Hybrid combination of NSM and CFRP wrapping	Concrete crushing, delamination of concrete cover, buckling of longitudinal rebar	Increase in load-carrying capacity by 16% for hybrid technique when compared to original specimen
Liu and Li [132]	RC columns under axial compression	Impressed current method (3% NaCl)	PEN fiber strengthening and CFRP wrapping	Rupture of CFRP composite	Enhancement in strength by 99.3% and 66.7% for PEN and CFRP strengthening techniques, respectively.
Li et al. [133]	RC beams under three-point bending	Impressed current method (3% NaCl)	FRP laminates	Debonding of CFRP strips	Increase in shear strength by 28.5% for 5% corrosion level
Kreit et al. [134]	RC beams subjected to three-point bending test	Salt spraying (35 g/L of NaCl)	Near-surface mounting using CFRP rod	Concrete crushing, debonding of NSM-CFRP rod, rupture of resin	Increase in stiffness by 10% No enhancement in strength or ductility observed
Al-Hammoud et al. [135]	RC beam subjected to three-point bending	Salted concrete (2.5% cement)	CFRP wrapping	Concrete crushing, rupture of CFRP sheets	Increase in fatigue strength by 28% and 20% for 10% and 15% corrosion levels, respectively.
Xie et al. [136]	RC beams subjected to four-point bending	Impressed current method (3% NaCl)	Repair using polymer mortar and CFRP wrap	Concrete crushing, breaking of CFRP sheets, debonding of CFRP strips	Increase in strength by 57.1%, 16.3% and 98.8% for CFRP wrap (only), combined polymer mortar repair + CFRP wrap and bonded CFRP, respectively
Al-Majidi et al. [137]	RC beams subjected to four-point bending test	Impressed current method (5% NaCl)	PVA and steel fiber-based GPC	Debonding and crushing of PVA-FRGPC, occurrence of shear failure in SFRGPC	Increase in load-carrying capacity by 50% for PVA-FRGC-strengthened specimen
Fang et al. [138]	RC columns under axial compression	Impressed current method (5% NaCl)	Alkali-activated slag mortar and stainless steel wire mesh (SSWM)	Cracking of ferrocement jacket, crushing of mortar inside SSWM	Increases in load-carrying capacity by 37%, 38% and 72% and increases in ductility by 77%, 44% and 79%

Table 2. Cont.

Reference	Specimen and Load Type	Corrosion Type	Repair Method	Intensity of Damage	Enhancement Observed
Elghazy et al. [139]	RC beam subjected to four-point bending test	Impressed current method (5% NaCl)	PBO-FRCM and CFRP laminates	FRCM delamination and slippage, CFRP rupture	Increases in strength by 105–144% and 130–152% for PBO-FRCM and CFRCM laminate-strengthened specimens
Hou et al. [140]	Bending test	Impressed current method (3.5% NaCl)	UHTCC	combined splitting and pull-out mode	Reduction in bond strength up to 13% for beams with medium levels of corrosion
Zhu et al. [141]	RC stub column under axial compression	Solution prepared with 3% chloride powder	Impressed current cathodic protection structural strengthening (ICCP-SS scheme)	Cracking of cementitious matrix, rupture of carbon fiber mesh in hoop direction	Increase in strength by 27.4% with the application of 80 mA/m ² current density

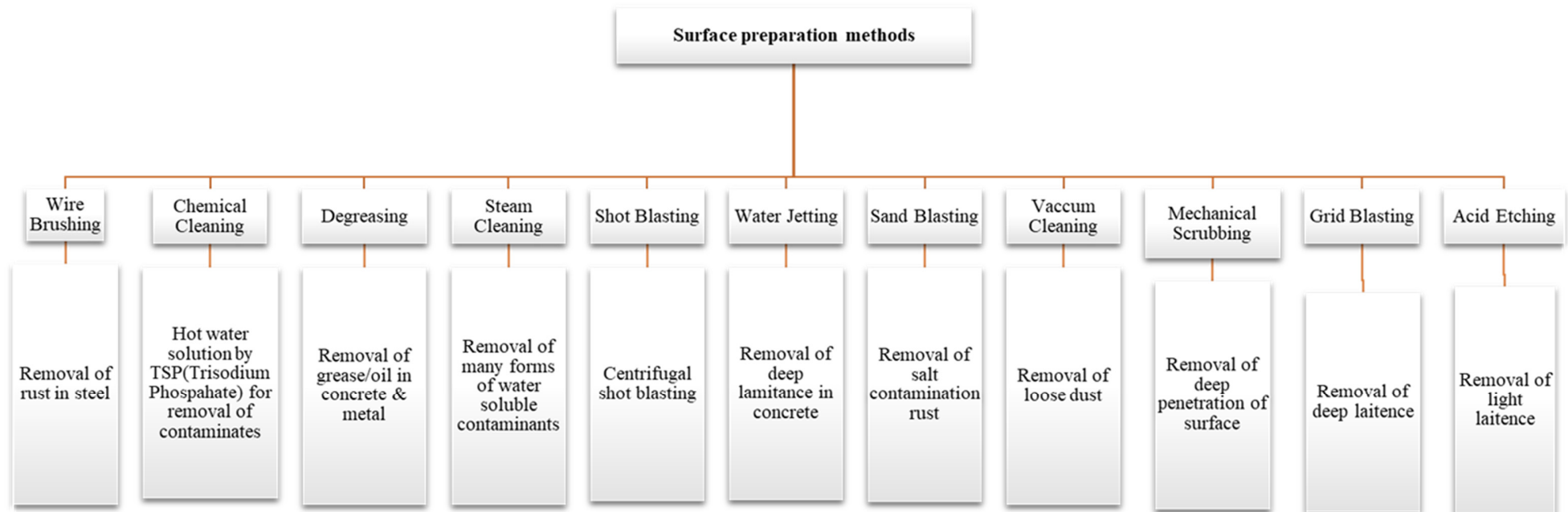


Figure 13. Surface preparation methods required prior to strengthening.

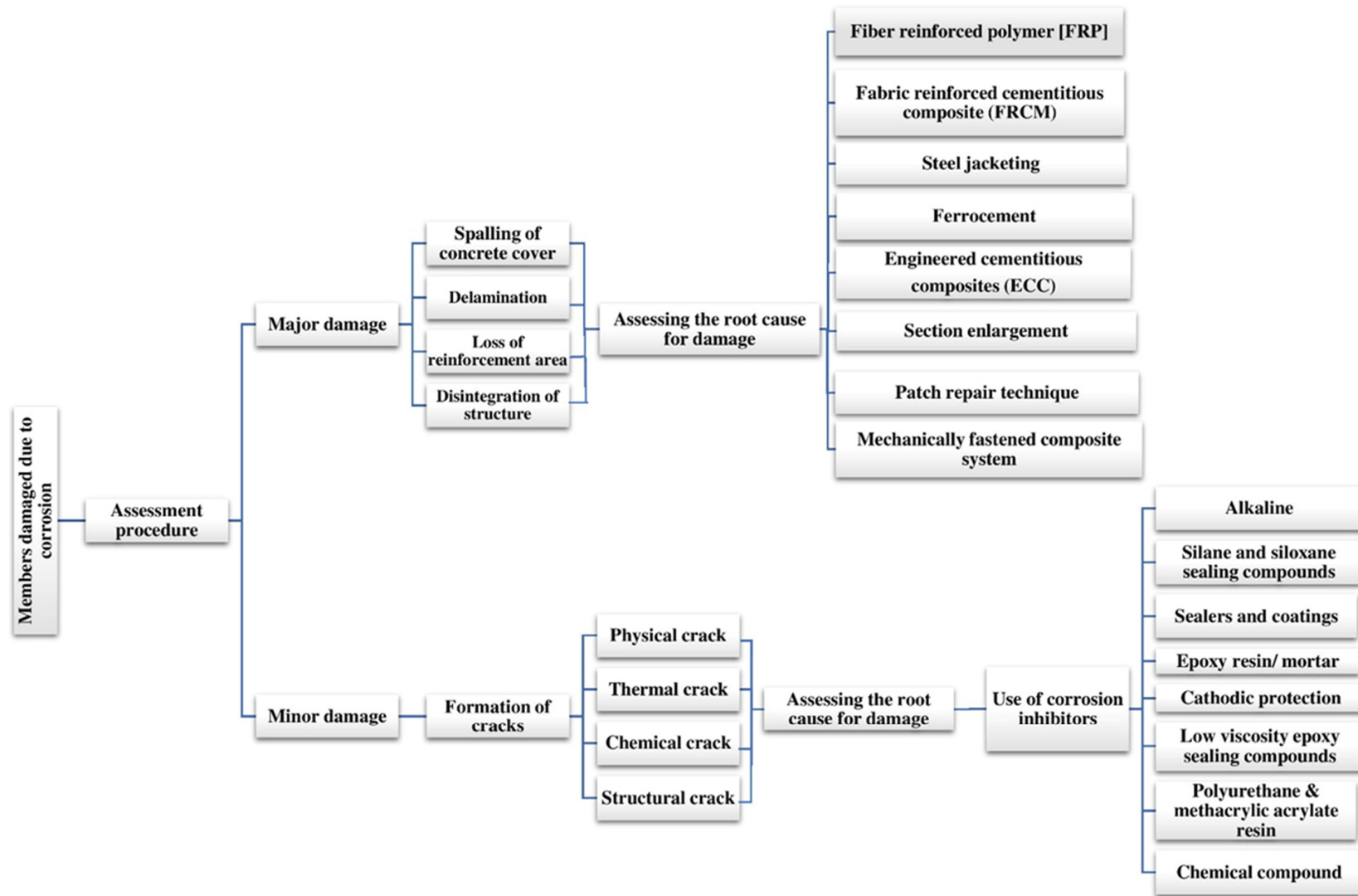


Figure 14. Assessment procedure for corrosion-damaged RC structures.

5.1. Steel Jacketing

Steel jacketing is one of the oldest strengthening methods developed for enhancing the confinement effect or flexural capacity of substantial/deficient RC members. This method uses steel plates to encase the deficient members and the gap is filled with non-shrink grout. In the past, a few studies have evaluated the efficacy of the steel plate bonding technique for enhancing the overall capacity of corrosion-damaged reinforced concrete members [142–145]. Salah et al. [146] studied the axial behavior of corroded RC columns strengthened using the steel jacketing technique. They added that the efficiency of steel bonding depends on the concrete substrate and the treatment of the corroded beams. First, the corroded cover concrete should be removed and rebars should be cleaned with a sand compressor or wire brush. This process is followed by grinding, roughening and bonding of the steel jacket to the substrate to achieve the desired performance. It is worth noting that the surface of the steel jacket should be coated using epoxy to avoid any further corrosion issues. To ensure better connections, steel angles can be used in the inner and outer re-entrant column corners and steel battens with a section size of 80 mm × 8 mm to connect the vertical elements of the steel jacket. The gaps should then again be filled with epoxy to ensure better bonding performance. As shown in Figure 15, the steel jackets are encased around the column and the gaps are filled with cementitious grout. Due to the high Young's modulus, the steel jacketing technique is highly efficient in carrying a large portion of the axial load in columns. However, the steel jacketing technique is vulnerable to corrosion and is not ideal for repairing RC members located in harsh marine environments.



Figure 15. Steel jacketing strengthening process. Adapted from [144].

5.2. Fiber-Reinforced Polymer Composites

In earlier times, strengthening of structural elements subjected to seismic damage was achieved by using concrete jacketing, enhancing the flexural and shear strengths of the damaged structures [147]. In recent times, the concrete enlargement technique is not preferred due to certain drawbacks, such as increased repair time, increases in dead weight, etc. Hence, the use of advanced composites, such as fiber-reinforced polymers (FRPs), has gained attention over the past two decades. The use of FRPs for static or seismic strengthening helps in improving the strength, stiffness and energy dissipation of RC structures [148–150]. FRP strengthening is performed either in the form of external bonding (the EB method) or by embedding the reinforcement in the cover of RC members in the form of the near-surface mounting (NSM) method.

The external bonding (EB) of FRP jackets has been successfully demonstrated over the past three decades and can improve the axial capacity of reinforced concrete members [151]. However, the EB technique requires careful preparation of the substrate since it is a contact-critical method; i.e., the technique relies on the contact with the parent stratum to achieve the desired performance. ACI 440.2R [152] specifications are followed for the strengthening of deficient RC members. The near-surface mounting (NSM) method has also been successfully used to enhance the bending and shear capacities of RC members [153].

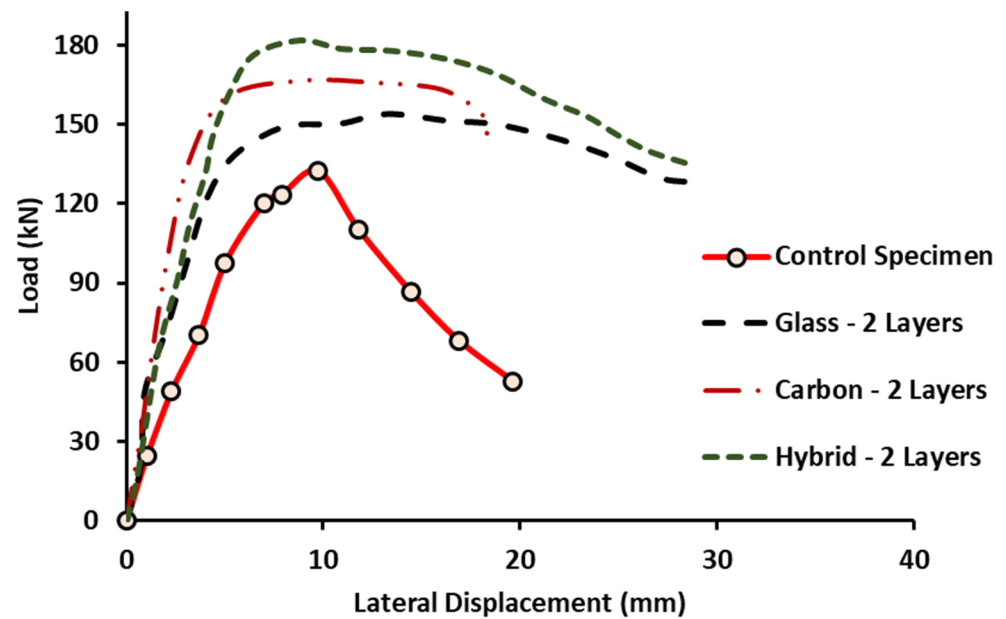
NSM involves the installation of additional longitudinal/transverse reinforcements to enhance bending and shear capacities, respectively. One major advantage of using NSM is the absence of surface preparation, as it is a bond-critical method [154–156]. For the selection of the dimensions of the groove, the size of the groove should be at least 1.5 times the diameter of the FRP reinforcement to achieve the desired strength enhancement [152]. As a matrix medium, materials such as epoxy resins, cement grout and paints can be utilized in the grooves to bond the NSM reinforcement to the concrete. After performing the strengthening procedure, a minimum curing time of 48 h is essential before the application of an external load. In recent times, a new hybrid FRP strengthening technique has been adopted to improve the load-carrying capacity of specimens. This hybrid technique is a combination of external bonding and the near-surface-mounted FRP method [157–162].

Results and Failure Mode Observations

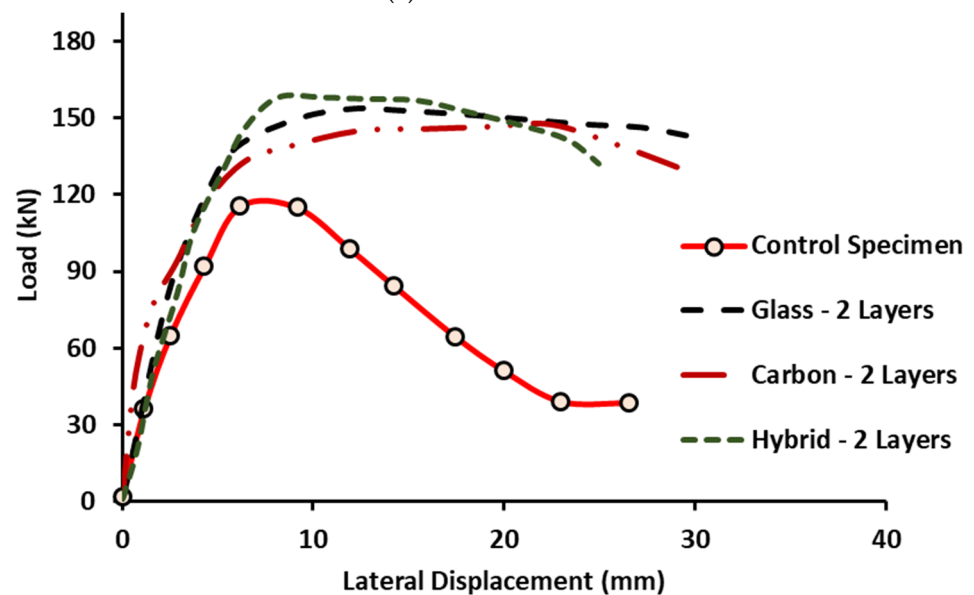
According to the literature review, the majority of investigators have focused on the flexural strengthening of corroded RC structures using carbon FRPs. NSM FRP strengthening is effective even when the deteriorated concrete cover is not repaired. Yousefi et al. [122] employed four layers of CFRP wrapping for the strengthening of a circular hollow steel column. When compared to the reference member, the strengthened specimen showed an enhancement in load-carrying capacity by 33.9% under axial compression loads. Moreover, CFRP confinement helped in improving the ductility by delaying the local buckling of steel and reduced the stress intensity in the corroded area. Haddad et al. [17] strengthened corroded RC beams with a combination of CFRP strips and CFRP sheet anchors. This combination of strips and an anchorage system resulted in the enhancement of the load-carrying capacity and flexural stiffness by 37% and 54%, respectively. Siad et al. [112] concluded from their experimental results that the use of CFRP sheets on the three faces of a beam (U-wrap) increased the ultimate strength by 60.2% when compared to the unstrengthened specimen. Moreover, it was also observed that the use of three-face wrapping prevented the occurrence of rapid debonding failure. Radhi et al. [130] observed an increase in the axial strength and ultimate strain levels of corroded circular RC columns using two layers of CFRP confinement. Moreover, they recommended increasing the number of layers of CFRP confinement for high corrosion levels so that the lost strength and ductility can be restored. Lee et al. [126] retrofitted large-scale RC columns using the CFRP sheet technique. Under axial compression loading, increases in the strength and ductility of 50% and 28%, respectively, were observed for corroded specimens. El-Maaddawy and Soudki [127] used CFRP strengthening to enhance the performance of corroded RC beams. They observed increases in the ultimate strength of up to 73% when compared to the unstrengthened RC specimens. Chotickai et al. [18] concluded that the volumetric CFRP ratio is a key parameter that greatly influences the performance of corrosion-damaged RC columns. Tigeli et al. [21] used a combination of the cementitious patch repair and CFRP laminate techniques to strengthen corroded RC beams. They concluded that the combined use of patch repair and CFRP laminates resulted in increases in the stiffness and ultimate load-carrying capacity of 25% and 50%, respectively. Jagtap et al. [14] used CFRP laminates to enhance the strength performance of corroded RC members. Test results revealed that strength of an augmented I-beam with CFRP laminate exceeded the original strength of reference beam by 162%. Joshi et al. [110] concluded from their studies that the use of GFRP confinement helped in enhancing strength by 129%, irrespective of corrosion degree, under uniaxial compression loading.

Jayaprakash et al. [20] experimentally compared the strengthening efficiency for mildly and severely corroded RC columns. The columns, which were subjected to corrosion for periods of 3 weeks (mild) and 6 weeks (severe), were strengthened with hybrid (CFRP + GFRP) and non-hybrid (CFRP and GFRP as separate layers) combinations. Figure 16 presents the data for the mild and severely corroded RC circular columns strengthened with different FRP techniques. It was observed that the use of the hybrid strengthening system enhanced the stiffness and strength of the columns when compared to those of

the non-hybrid wrapping schemes. Figure 16b shows that both hybrid and non-hybrid strengthening layers increased the ductility of the severely corroded columns compared to the unstrengthened corroded specimens. Other than CFRP strengthening, Ray et al. [125] used FRP retrofitting with two different substrate techniques: polymer-modified repair mortar composite (PMC) and crack filling only (CFO). They concluded that CFO FRP strengthening restored the strength lost when compared to the PMC FRP-repaired beams. However, the PMC-repaired specimens exhibited higher ductility than the CFO FRP system.



(a) Mild corrosion



(b) Severe corrosion

Figure 16. Load versus displacement curves for mild and severely corroded RC columns with and without FRP strengthening. Reproduced from [20].

The researchers also used FRP strengthening to restore the seismic performance of corroded RC elements. Shen et al. [119] strengthened a corroded shear wall using BFRP confinement and tested it under quasi-static cyclic loading. At 3% and 9% corrosion levels, basalt fiber-reinforced polymer (BFRP) jackets were able to regain the original drift levels.

However, a similar performance enhancement was not observed for the specimens with a 15% corrosion level. Jia et al. [111] used CFRP strengthening for reinforced columns with low-level corrosion under quasi-static cyclic loads. Although CFRP jackets boosted the energy dissipation capacity and decreased the intensity of concrete crushing and longitudinal rebar buckling, the test findings revealed that this strengthening technique did not improve the lateral strength of the corroded columns.

Siddika et al. [163] experimentally investigated the behavior of corroded I beams strengthened using GFRP composites. The test results revealed that the use of GFRP resulted in better energy absorption properties and was more suitable for earthquake-prone areas. Moreover, it was inferred from the overall review that materials such as glass and carbon fiber-reinforced polymer led to better dissipation capacities. Li et al. [164] used a combination of CFRP wraps and the steel jacketing technique with four angles welded by batten plates, which resulted in better seismic performance in a corroded RC stub column. Moreover, this combination enhanced the stiffness, energy dissipation capacity and ductility by 16.7%, 23.3% and 14.9%, respectively, compared to the single strengthening technique.

5.3. Ferrocement Technique

The ferrocement technique is one alternative strengthening/repair technique when the use of the chemical-based FRP technique is not feasible. The ferrocement technique employs steel wire mesh, which is closely spaced and acts as the reinforcing material. The matrix phase is prepared with rich cement mortar with proportions of 1:3 or 1:2. The w/c ratio of the mortar is kept as low as 0.40 to avoid cracking due to shrinkage issues. Ferrocement jacketing can be applied with the following methods: (a) hand plastering, (b) a semi-mechanized process, (c) centrifuging and (d) a guniting process. After the process, an orbital vibrator is used to the compacting of ferrocement layers uniformly. This ferrocement technique is used to improve the performance of corrosion-damaged RC members. Jayasree et al. [44] investigated corrosive specimens and classified them based on the intensity of corrosion as less corroded (5%), moderately corroded (10%) and severely corroded (15%) specimens. They then strengthened them using ferrocement jacketing. It was inferred that the less and moderately corroded specimens had their original load-carrying capacities restored using this technique, as shown in Figure 17. It was also recommended to provide an additional layer of mesh reinforcement to restore the load-carrying capacity in severely damaged specimens.

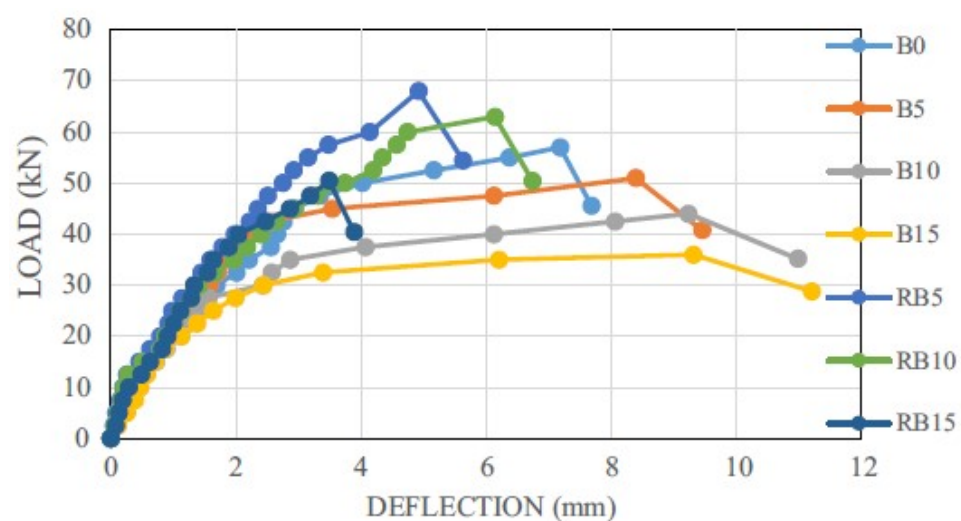


Figure 17. Load–deflection curves with ferrocement retrofitting scheme. Reproduced with permission from [44], Elsevier, 2016. Note: B and R represent control and retrofitted specimens with 0%, 5%, 10% and 15% corrosion levels.

5.4. Patch Repair Technique

Patch repair is the process of cleaning corroded steel and replacing the deteriorated concrete cover with new mortar. Alwash et al. [115] developed a novel patch repair technique for strengthening corroded RC beam–column elements. In this technique, the existing concrete cover damaged due to corrosion is removed and cleaned with an air blower. For low corrosion levels (e.g., less than 20% loss in rebar area), a drill motor with a brush is used to clean the bar. For corrosion levels exceeding 20%, the corroded bit is cut and removed before being replaced with a new steel bar of the same diameter with the overlap length. After the cleaning process, epoxy-based primer is applied on the surface to increase the bonding capacity of the substrate. Then, non-shrink cement mortar is applied to replace the damaged concrete layer. The authors concluded that the load-carrying capacity of rehabilitated specimens was enhanced by 95.5% and 97.3% and decreases in ductility by 19% and 15% were observed for corrosion levels of 5% and 20%, respectively.

5.5. Fabric-Reinforced Cementitious Matrix (FRCM)

Glass, carbon and polyparaphenylene benzobisoxazole (PBO) are some of the dried fabrics embedded in the cement-based matrixes used to produce FRCMs [165]. The first step is to remove the corrosion-damaged portion of the concrete with a hydraulic hammer or other equipment and then brush away the rust. After that, the beam should be repaired using local mortar and allowed to cure for seven days. Then, sandblasting should be undertaken to roughen the surface of the prepared beam. After that, it is left to soak in water for around 2 h. Then, an initial coat of cementitious matrix is applied, followed by the installation of fabrics. The process is repeated until the desired number of layers is obtained. Adding more FRCM layers helps to increase the yielding and ultimate loads of the specimen. Elghazy et al. [41] employed PBO-based FRCM and carbon FRCM methods to repair corroded beams. They followed ACI 549.4R-13 for the hand lay-up approach. The strengthening procedure for FRCM is shown in Figure 18.

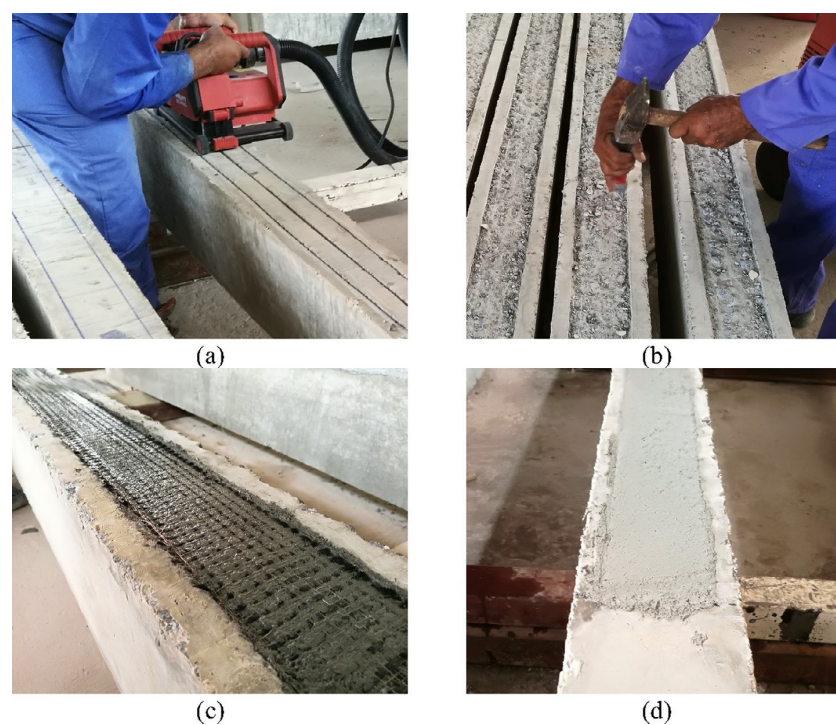


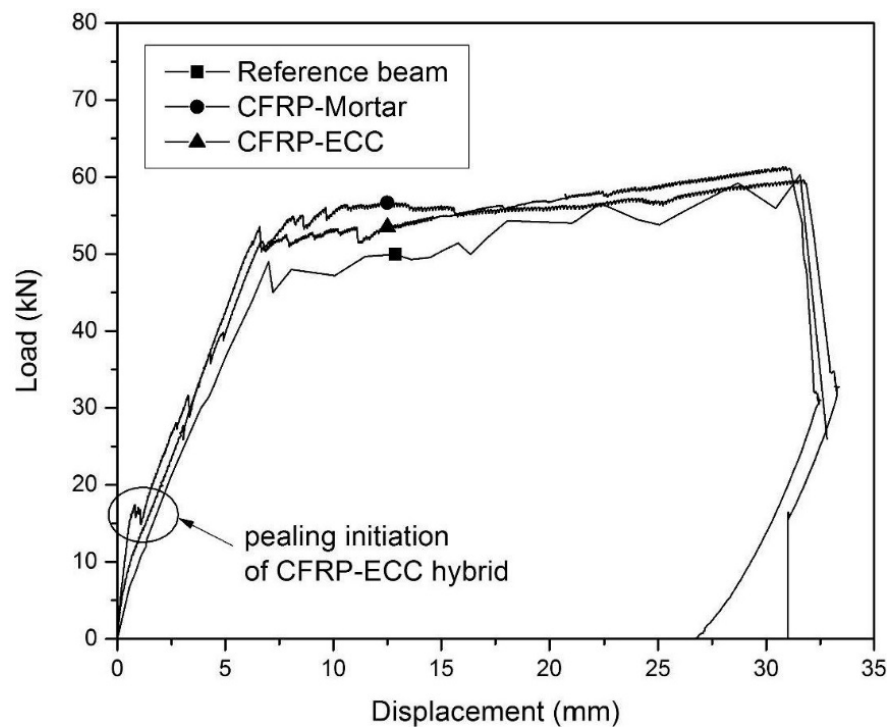
Figure 18. FRCM strengthening process: (a) grooving the beam, (b) chipping the concrete and clearing the groove, (c) applying first layer of mortar and impregnating the fabric, (d) finishing after FRCM application. Reproduced with permission from [39], Elsevier, 2019.

As found in the literature review, Elghazy et al. [139] used phenylene benzobisoxazole-based FRCM and carbon FRCM to strengthen corrosion-damaged RC members. They reported that the C-FRCM restored load-bearing capacity by 152 percent whereas PBO-FRCM restored only 144% of the original capacity. Moreover, C-FRCM showed a higher post-yielding stiffness than PBO-FRCM. They also stated that the U-wrapped FRCM scheme was more effective than the bottom-end-anchorage solution in increasing the ultimate load-carrying capacity. Zhu et al. [141] retrofitted RC stub columns with a combination of ICCP and CFRCM strengthening techniques. According to them, this combination of two different strengthening (SS) strategies increased the compressive strength more than the individual strengthening method. They also highlighted that the combined strengthening technique is a suitable solution for RC structures located in regions with extreme environmental conditions.

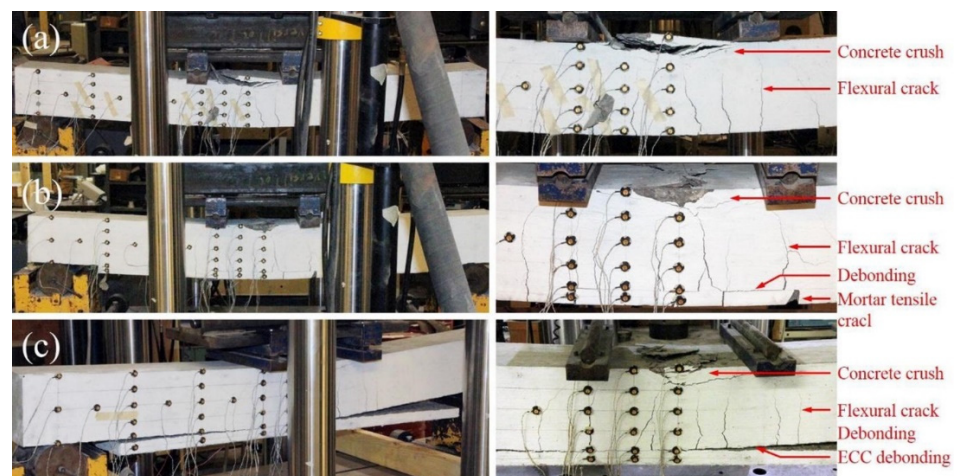
Elghazy et al. [41] used CFRCM strengthening for corroded RC members. A 65% increase in the flexural strength was witnessed compared to the control specimen. They concluded that the U-wrapped technique is more efficient than the end-anchorage scheme in preventing FRCM ply delamination failure. Elghazy et al. [37] used two different externally bonded composite strengthening systems, polyparaphenylene benzobisoxazole fabric-based (P-FRCM) and carbon sheet (C-FRCM) composites, to strengthen corroded RC beams. P-FRCM composites use a polymer-modified cementitious matrix (PFMC) as a matrix along with polyparaphenylene benzobisoxazole (PBO) fibers as the reinforcement. The experimental findings indicated that both the strengthening techniques increased the load-bearing capacity of the beam compared to its original strength. Moreover, the authors added that the use of CFRP composites was more efficient in restoring the flexural strength than the PFRCM system.

5.6. Engineered Cementitious Composites

ECCs are high-performance fiber-reinforced cementitious composites that enhance ductility when compared to the conventional concrete available commercially. This high ductility is characterized through its strain hardening response in tension stress–strain curves, and the failure strain increases by 50 times compared to conventional concrete. In earlier days, different cementitious materials, such as fly ash, slag and micro-silica, were mixed with concrete to mitigate corrosion [166–168]. Hence, use of ECCs has been successful in the past for the repair and rehabilitation of damaged RC members or construction of new structural elements when ductility is of paramount importance. In addition to the ductility, ECCs also possess better strength characteristics, with a minimum compressive strength of 30 MPa. Wu et al. [51] studied two types of strengthening schemes for corrosion-damaged RC beams. The first was a hybrid combination of mortar and CFRP wrapping and the second was a hybrid CFRP-ECC strengthening scheme. The load-displacement curves for the two specimens strengthened using the different schemes and the reference specimen obtained from the four-point bending test are shown in Figure 19i. Strengthening using a hybrid CFRP-ECC combination helped in increasing the load-carrying capacity ($P_u = 61.3$ kN) compared to the hybrid CFRP wrapping system ($P_u = 59.6$ kN). The failure modes of the reference specimen and the corrosion-strengthened specimens are presented in Figure 19ii.



(i) Comparison of load–displacement curves



(ii) Comparison of failure modes

Figure 19. Comparison of strengthening efficiency with different FRP techniques. Reproduced with permission from [51], Elsevier, 2017. Note: (a) reference beam, (b) beam with CFRP mortar hybrid strengthening, (c) beam with CFRP-ECC hybrid strengthening.

As found in the literature survey, Sahmaran et al. [128] compared the corrosion mechanisms in a mortar specimen and ECC prism made with a centrally placed deformed bar. The test results revealed that the strength of the mortar specimen decreased by 34% after 25 h of corrosion, but the ECC specimens showed almost 100% flexural capacity, as high as the control specimens, after 50 h of accelerated corrosion exposure. Hu et al. [50] used a hybrid CFRP-ECC strengthening system to restore stiffness, strength and bond behavior in corroded RC beams. They concluded that excessive provision of the ECC layer resulted in marginal enhancements to the flexural performance of the beam. Due to its outstanding crack-restraining capabilities and multiple types of cracking behavior, ECCs have been termed the “crack relief layer (CRF)”.

Zheng et al. [43] researched the effects of different parameters, such as FRP grid types, strengthening amounts, corrosion levels and longitudinal ratios, on the flexural strengthening of corrosion-damaged RC beams via an FRP grid (carbon and basalt)-reinforced ECC matrix. The results indicated that the maximum percentage increases in the flexural strength for CFRP and BFRP were 62.0% and 47.3%, respectively. Zheng et al. [49] studied the strengthening efficiency of corrosion-damaged RC beams using FRP grid-reinforced ECCs. The test results highlighted that the shear strength of the strengthened beam ranged from 12.4% to 36.4%. Furthermore, the flexural stiffness of the beams with corrosion-damaged stirrups increased to a certain extent when using this strengthening technique. Similar observations were noted in other studies on the shear behavior of corroded RC beams with FRP grid-reinforced ECCs [48–51]. Hou et al. [42] used an ultra-high-toughness cementitious composite (UHTCC) repairing technique for the strengthening of corroded RC beams. During the strengthening procedure, the rust from the corroded rebar was removed using a steel brush. Further, the surface was roughened using a tilting hammer. Following that, a UHTCC repair layer was applied over the surface of the concrete. For heavily corroded stirrups, CFRP strips and anchorages were placed over the UHTCC layer. After the necessary curing process, the strengthened specimens were tested under static or seismic loading. The test results showed that there was an increase in the load-carrying capacity for the corrosion ratio of 11.2%. The authors found that the UHTCC-strengthened specimen showed better tensile behavior, durability and crack control capacity in the repair and strengthening of RC members, particularly in marine environments.

5.7. Mechanically Fastened Composites

EI-Maaddawy et al. [129] employed a pultruded FRP composite, which is a hybrid combination of carbon and glass fibers, with a vinyl ester matrix to strengthen a corrosion-damaged RC beam. Prior to the FRP composite plate installation, the stratum was cleaned with powered actuated fasteners (PAFs), which are powder-actuated guns. To avoid surface damage or cracking of the concrete, holes should be predrilled at the locations where fasteners will be installed. After that, expansion anchor bolts (EABs) were installed with a rotary hammer drill using washers, nuts and tilting-hammer threaded anchor bolts (TABs). The test results revealed that using the EAB and TAB fastening system enhanced strength by 81%–85% and using the PAF strengthening scheme led to an enhancement of 67%. As shown in Figure 20, strengthening of a damaged specimen using a mechanically fastened composite was performed by Zhang et al. [167] in addition to detailed nonlinear FE analyses. The nonlinear finite element analysis was performed using ABAQUS software in order to predict the load distribution for the bolts and to identify the maximum compressive strain at the point of impact in the strengthened specimen.

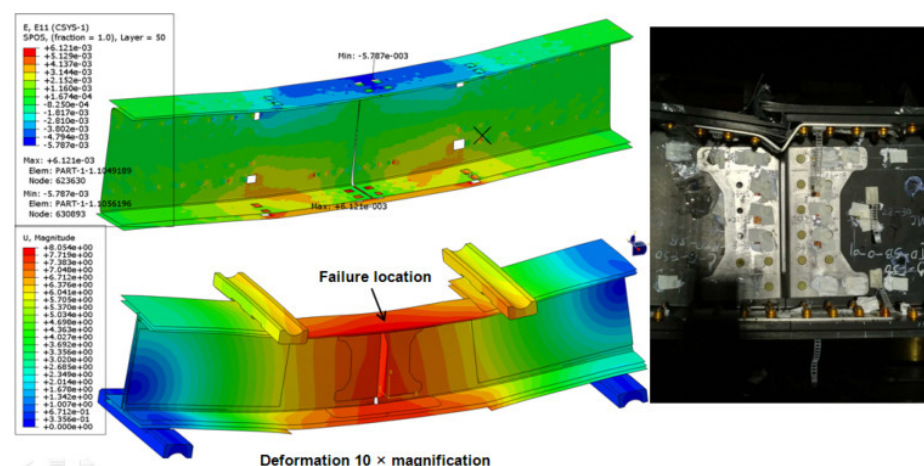


Figure 20. Morphologies of failure modes for composite C-beam fastened with multi-bolt joints. Reproduced with permission from [167], Elsevier, 2019.

5.8. Impressed Current Cathodic Protection (ICCP) Repair Technique

Neutralizing the electrochemical activity of concrete reinforcement corrosion is referred to as the impressed current cathodic protection (ICCP) technique. Zhu et al. [141] used a 3 mm thick carbon mesh composed of cementitious matrix to implement the ICCP process on the surface of a beam. The corroded beam was neutralized by connecting the rebar and carbon mesh to a multi-channel direct current supply with the current densities of 26 mA/m^2 and 80 mA/m^2 , respectively, with the rebar and carbon mesh operating as the cathode and anode. The schematic of the ICCP setup for corroded RC members is shown in Figure 21.

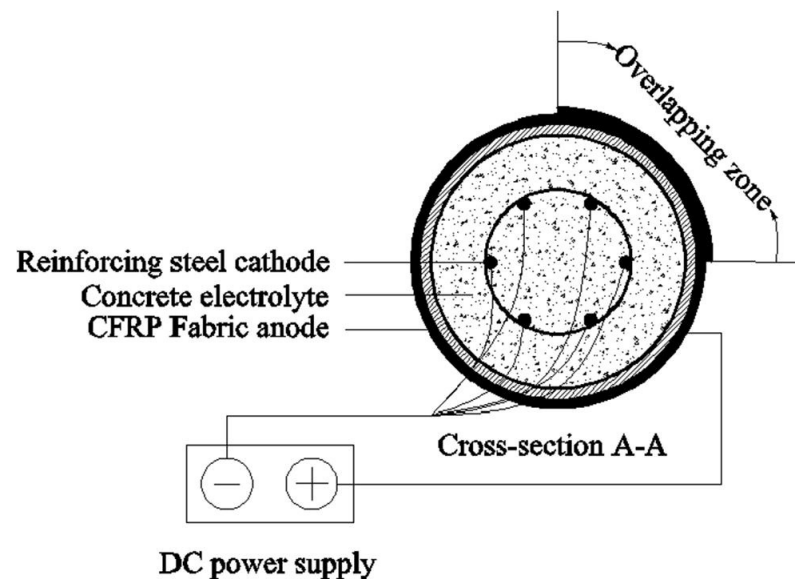


Figure 21. Schematic of ICCP for corroded RC members. Reproduced with permission from [141], Elsevier, 2018.

A compression test was performed after the corrosion treatment process with the ICCP-repaired column and reference specimen. The ICCP-repaired specimen could carry a maximum load of 1605 KN, while the reference specimen had a load-carrying capacity of 1545 KN. Furthermore, the ICCP-repaired column strengthened with carbon mesh exhibited an increase in compressive strength of 16.7%. After the compression test, the rebar was tested for the corrosion levels. It was concluded that, after 100 days of ICCP treatment, no corrosion products could be identified. However, it is worth noting that this approach is not suitable for specimens containing sodium chloride.

5.9. Performance Comparison of Strengthening Techniques for Corroded RC Members

The critical review of the efficiency of different strengthening methods in restoring the performance of corrosion-damaged reinforced concrete (RC) members was analyzed. Figure 22 provides a statistical comparison of the improvements attained using different strengthening methods; however, the effectiveness of the proposed strengthening methods depends on several other external factors, such as (a) the compressive strength of the original strata, (b) member size, (c) the extent of the damage in terms of mass loss in the steel reinforcement, etc. However, their effects are minor when compared to the other important parameters and were ignored when undertaking the comparison.

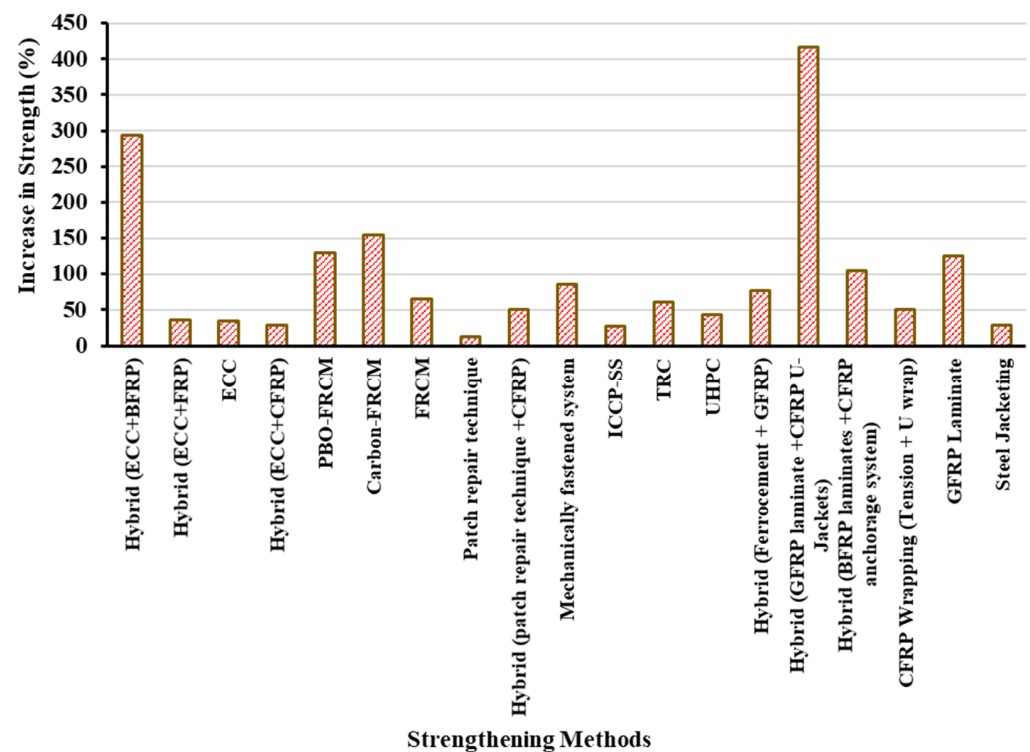


Figure 22. Comparison of strength enhancements using various strengthening techniques.

Among the different strengthening methods proposed, the FRP technique was found to perform well in increasing ultimate strength compared to unstrengthened members. Hence, the majority of previous researchers used the FRP strengthening technique to restore the strength of corroded RC structures. Furthermore, different types of fibers, such as carbon, basalt and glass fibers, have been employed and conventional epoxy resin can be used for the matrix component. In the comparison of these techniques, it was found that the hybrid FRP technique combining GFRP and CFRP achieved the maximum load-bearing capacity of 417%. Secondly, the ECC and BFRP techniques showed increase in load-carrying capacity of nearly 300%. Thirdly, GFRP laminates, PBO-FRCM and carbon-FRCM demonstrated load-carrying capacities of 100–150%, while a few techniques, such as steel jacketing, the patch repair technique, UHPC, ICCP-SS, mechanically fastened systems and textile-reinforced concrete, were found to be least preferable due to poor performance (<25%). It can also be noted that strengthening with FRPs was the most substantial technique for corrosion, and more than 40% of researchers used FRPs either as a single substantive layer or as a hybrid layer.

6. Design Recommendations and Conclusions

6.1. Design Recommendations for Further Investigations

This study presents a detailed analysis of the state-of-the-art knowledge on the repair and strengthening of severely corroded reinforced concrete elements under both static and dynamic loading conditions. The various topics elaborated in detail and discussed included (a) the corrosion mechanism of concrete reinforcement; (b) methods of generating corrosion in structural elements; and (c) procedures and materials for the repair and strengthening of corroded RC members, such as fiber-reinforced polymers, engineered cementitious composites, steel jacketing, mechanically fastened composites, ultra-high-performance cementitious composites, the patch repair technique, fabric-reinforced cementitious composites and the ferrocement technique. Though the efficiency of strengthening techniques has been proved by different researchers, it is essential to understand the mechanism of corrosion and the quantitative aspect of the damage that arises so that optimistic design

solutions can be provided. However, the performance enhancements of different techniques are also dependent on several parameters, such as (a) the type of loading (flexure, shear, compression, etc.), (b) the bond between the parent member and the strengthening solution used, (c) the intensity of corrosion damage, etc. Based on the understanding of the effects of corrosion resulting from different artificial corrosion-inducing mechanisms and the techniques to enhance their performance, the following generic design recommendations can be proposed:

- Among the different corrosion-inducing techniques, the accelerated corrosion process (ACP) could yield the desired corrosion levels with a shorter time period and a low initial setup cost. To achieve a low or medium corrosion level (i.e., mass loss < 10%), three critical design parameters—current density, time and concentration of NaCl—should be set as $60 \mu\text{A}/\text{cm}^2$, 30 days and 3.5%, respectively. In order to achieve high levels of corrosion damage in reinforced concrete sections, a minimum current density of $200 \mu\text{A}/\text{cm}^2$ should be maintained. In addition, the duration of the corrosion induction and the concentration of NaCl solution play key roles and should be maintained at the minimum values of 30 days and 3.5%, respectively;
- For the strengthening of low or moderately damaged RC members, the combined use of a patch repair system and fiber-reinforced polymer composite reinforcement ($\rho_f = 1.5\%$) may be helpful in completely restoring strength and ductility. The use of single strengthening systems, such as FRCM or ECCs, can be highly effective for members with moderate damage levels. However, the selection of fibers plays a key role. Carbon- or PBO-based FRCMs can be highly effective and achieve 100% enhancements in load-carrying capacity. However, their application in the field may be limited by their high initial cost;
- The use of a hybrid ECC or FRCM system is essential to restore the lost performance of heavily corroded RC members where the total mass loss is more than 15%. In such a scenario, the minimum thickness of the ECC layer to be provided is 25–30 mm beyond the concrete cover, and the minimum longitudinal reinforcement ratio is 1.0%;
- For both individual and hybrid strengthening schemes, the use of dowel connections or FRP anchors to bond the existing strata and new stratum can help in yielding the desired performance enhancements under shear or combined shear and flexure load combinations.

6.2. Summary and Conclusions

The following conclusions can be derived based on the findings summarized as part of this work:

1. Among the various corrosion-inducing methods, the accelerated corrosion method using NaCl solutions of 3%, 3.5% and 5% was found to be more extensively used by researchers. Other techniques for inducing corrosion were rarely selected due to the cost and easiness of developing corrosion similar to that from real-time observations;
2. Among the strengthening methods discussed, the FRP and ECC methods were the most extensively used strengthening techniques for corrosion-damaged RC members, and they were found to be able to restore materials' original capacity. A few researchers utilized steel jacketing and mechanically fastened systems. However, the durability of members located in harsh environmental conditions is a point in question;
3. For corroded RC members subjected to dynamic seismic loading, the use of ECC and FRP strengthening resulted in better energy dissipation capacities and lateral strength enhancement compared to other techniques. Moreover, a combination of CFRP wraps and steel jacketing resulted in enhancement of the strength and ductility;
4. The hybrid strengthening scheme using FRP-ECCs and FRCM with U-wrapping enhanced flexural performance to a significant level compared to single strengthening techniques;
5. Though the effects of different corrosion-strengthening procedures are well-established, their long term performance and effectiveness are points of concern or have not been

studied extensively. Hence, it is important to understand the durability properties of different strengthening systems and this will be the aim of further investigations.

Author Contributions: Conceptualization, U.B. and M.C.; Methodology, U.B., J.M., M.C. and N.A.; Formal analysis, U.B.; Investigation, J.M., M.C. and N.A.; Writing—original draft, U.B.; Writing—review & editing, J.M., M.C. and N.A.; Visualization, J.M.; Supervision, M.C. All authors have read and agreed to the published version of the manuscript.

Funding: This research received no external funding.

Data Availability Statement: Not applicable.

Conflicts of Interest: The authors declare no conflict of interest.

Nomenclature

A	exposed specimen area, cm^2
$A_0(x)$	initial cross-sectional area along the bar length x , documented before beam casting
$A_{\text{fin}}(x)$	final cross-sectional area along the bar length x , evaluated after the structural failure test
A_m	atomic mass (for iron, 55.85 g)
α	proposed correction/calibration factor for Faraday's law (or) target corrosion ratio
C_{Faraday}	Faraday's constant (96485 C/mol)
d	reinforcing steel bar diameter
d_b	diameter of reinforcing bar
D_1^c	original diameter of the number i -type rebar before corrosion testing
ρ	density of iron (7.85 g/cm^3)
ρ_w	corrosion rate
$\Delta A_{\text{yn}}(x)$	decrease in cross-section area caused by yielding and necking of the tensile bar
E_w	equivalent weight for pure metals
F	Faraday's constant (96,500 C/mol)
γ	rebar radius
i	current density
i_{cor}	corrosion current density, $\mu\text{A}/\text{cm}^2$
I	average current (A) applied over time increment Dt (s)
I_{cor}	total anodic current, μA
K_1	3.27×10^{-3} , $\text{mm g}/\mu\text{A cm yr}$
K_2	8.954×10^{-3} $\text{g cm}^2/\mu\text{A m}^2\text{d}$
l	corrosion length in steel bar
L	total length of reinforcements connected in series
Li	length of each rebar unit (in the present study, the unit length of each number 6 and number 4 rebar section was equal to 340 cm, while the unit length of the number 3 stirrup was $2 \text{ cm} \times 25 \text{ cm}$)
m	rebar mass loss
M	molar mass of iron (56 g/mol)
m_0 and l_0	initial mass and length of the non-corroded stirrups
m_1	initial mass of bar per unit length
m_1 and l_1	final mass and length of the corroded stirrups
m_2	mass of bar after the corrosion process
m_{loss}	targeted mass loss (grams)
MR	$\text{g}/\text{m}^2\text{d}$
m_{specimen}	molar mass of the reinforcement bar (55.8 mol)
m_t	mass loss in corroded reinforcement at target corrosion ratios (g)
μ_{avg}	actual average corrosion level

n	number of bars (or) number of electrons required to oxidize an atom of the element in the corrosion process
N _i	total number of number i-type rebar units (N ₆ = 2, N ₄ = 2, N ₃ = 34 in the present study)
η _s	percent mass loss in the design
r	radius of the steel bars (in mm)
ρ _l	ratio of longitudinal steel reinforcement
R	corrosion rate
S	total surface area of the reinforcement material within a specimen
t	corrosion duration (in sec) (or) time elapsed in hours after casting
W	atomic weight of the element
w(g)	accumulated steel loss (g)
z	number of electrons released when one iron atom is converted into an iron ion (equal to 2)
Z	valence in the corrosion reaction (+2)

References

1. Angst, U.M. Challenges and opportunities in corrosion of steel in concrete. *Mater. Struct.* **2018**, *51*, 4. [CrossRef]
2. Appendix A. Assessment of Global Cost of Corrosionl. 2015. Available online: <http://macroeconomics.kushnirs.org/index.php?area=germany&indicator=gdp&lang=en> (accessed on 23 December 2015).
3. Koch, G.H.; Brongers, M.P.H.; Thompson, N.G.; Virmani, Y.P.; Payer, J.H. *Corrosion Costs and Preventive Strategies in the United States*; Federal Highway Administration: Washington, DC, USA, 2002.
4. Liu, M. Corrosion and mechanical behavior of metal materials. *Materials* **2023**, *16*, 973. [CrossRef] [PubMed]
5. Xu, C.; Guo, C.; Xu, Q.; Yang, Z. The global collapse resistance capacity of a seismic-damaged SRC frame strengthened with an enveloped steel jacket. *Structures* **2021**, *33*, 3433–3442. [CrossRef]
6. Xu, C.X.; Peng, S.; Deng, J.; Wan, C. Study on seismic behavior of encased steel jacket-strengthened earthquake-damaged composite steel-concrete columns. *J. Build. Eng.* **2018**, *17*, 154–166. [CrossRef]
7. Adam, J.M.; Ivorra, S.; Pallarés, F.J.; Giménez, E.; Calderón, P.A. Axially loaded RC columns strengthened by steel caging. finite element modelling. *Constr. Build. Mater.* **2008**, *23*, 2265–2276. [CrossRef]
8. Adam, J.M.; Gimenez, E.; Calderon, P.A.; Pallares, F.J.; Ivorra, S. Experimental study of beam-column joints in axially loaded RC columns strengthened by steel angles and strips. *Steel. Compos. Struct.* **2007**, *8*, 329–342. [CrossRef]
9. Adam, J.M.; Ivorra, S.; Gimenez, E.; Moragues, J.J.; Miguel, P.; Miragall, C.; Calderon, P.A. Behaviour of axially loaded RC columns strengthened by steel angles and strips. *Steel. Compos. Struct.* **2007**, *7*, 405–419. [CrossRef]
10. Garzon-Roca, J.; Adam, J.M.; Calderon, P.A. Behaviour of RC columns strengthened by steel caging under combined bending and axial loads. *Constr. Build. Mater.* **2011**, *25*, 2402–2412. [CrossRef]
11. Chellapandian, M.; Prakash, S.S.; Sharma, A. Experimental and finite element studies on the flexural behaviour of reinforced concrete elements strengthened with hybrid FRP technique. *Compos. Struct.* **2019**, *208*, 466–478. [CrossRef]
12. Kaya, A.; Dawood, M.; Gencturk, B. Repair of corroded and buckled short steel columns using concrete-filled GFRP jackets. *Constr. Build. Mater.* **2015**, *94*, 20–27. [CrossRef]
13. Belarbi, A.; Bae, S.W. An experimental study on the effect of environmental exposures and corrosion on RC columns with FRP composite jackets. *Compos. B Eng.* **2007**, *38*, 674–684. [CrossRef]
14. Jagtap, P.R.; Pore, S.M. Strengthening of fully corroded steel I beam with CFRP laminates. *Mater. Today Proc.* **2021**, *43*, 2170–2175. [CrossRef]
15. Al-Saidy, A.H.; Al-Harthy, A.S.; Al-Jabri, K.S.; Abdul-Halim, M.; Al-Shidi, N.M. Structural performance of corroded RC beams repaired with CFRP sheets. *Compos. Struct.* **2010**, *92*, 1931–1938. [CrossRef]
16. Zhou, Y.; Chen, X.; Wang, X.; Sui, L.; Huang, X.; Guo, M.; Hu, B. Seismic performance of large rupture strain FRP retrofitted RC columns with corroded steel reinforcement. *Eng. Struct.* **2020**, *216*, 110744. [CrossRef]
17. Haddad, R.H. Hybrid repair configurations with CFRP composites for recovering structural performance of steel-corroded beams. *Constr. Build. Mater.* **2016**, *124*, 508–518. [CrossRef]
18. Chotickai, P.; Tongya, P.; Jantharaksa, S. Performance of Corroded Rectangular RC Columns Strengthened with CFRP Composite under Eccentric Loading. *Constr. Build. Mater.* **2021**, *268*, 121134. [CrossRef]
19. Kim, T.K.; Kim, S.H.; Park, J.S.; Park, H.B. Experimental evaluation of PSC structures from FRP with a prestressing strengthening method. *Materials* **2021**, *14*, 1265. [CrossRef]
20. Jayaprakash, J.; Pournasiri, E.; De’nan, F.; Anwar, M.P. Effect of corrosion-damaged RC circular columns enveloped with hybrid and non-hybrid FRP under eccentric loading. *J. Compos. Mater.* **2015**, *49*, 2265–2283. [CrossRef]
21. Tigeli, M.; Moyo, P.; Beushausen, H. Behaviour of corrosion damaged reinforced concrete beams strengthened using CFRP laminates. *RILEM Bookser.* **2012**, *6*, 1079–1085. [CrossRef]

22. Yang, J.; Haghani, R.; Blanksvård, T.; Lundgren, K. Experimental study of FRP-strengthened concrete beams with corroded reinforcement. *Constr. Build. Mater.* **2021**, *301*, 124076. [CrossRef]
23. Kalyoncuoglu, A.; Ghaffari, P.; Goksu, C.; Ilki, A. Rehabilitation of corrosion-damaged substandard RC columns using FRP sheets. *Adv. Mater. Res.* **2013**, *639–640*, 1096–1103. [CrossRef]
24. Kang, T.H.K.; Ary, M.I. Shear strengthening of reinforced & prestressed concrete beams using FRP, Part II-Experimental investigation. *Int. J. Conc. Struct. Mater.* **2011**, *6*, 49–57.
25. Badawi, M.; Soudki, K. CFRP repair of RC beams with shear-span and full-span corrosions. *J. Compos. Constr.* **2010**, *14*, 323–335. [CrossRef]
26. Li, P.; Ren, Y.; Zhou, Y.; Zhu, Z.; Chen, Y. Experimental study on the mechanical properties of corroded rc columns repaired with large rupture strain FRP. *J. Build. Eng.* **2022**, *54*, 104413. [CrossRef]
27. Karimipour, A.; Edalati, M. Retrofitting of the corroded reinforced concrete columns with CFRP and GFRP fabrics under different corrosion levels. *Eng. Struct.* **2021**, *228*, 111523. [CrossRef]
28. Kashi, A.; Ramezani pour, A.A.; Moodi, F. Durability evaluation of retrofitted corroded reinforced concrete columns with FRP sheets in marine environmental conditions. *Constr. Build. Mater.* **2017**, *151*, 520–533. [CrossRef]
29. Pan, T.; Zheng, Y.; Zhou, Y.; Liu, Y.; Yu, K.; Zhou, Y. Coupled effects of corrosion damage and sustained loading on the flexural behavior of RC beams strengthened with CFRP anchorage system. *Compos. Struct.* **2022**, *289*, 115416. [CrossRef]
30. Do-Dai, T.; Chu-Van, T.; Tran, D.T.; Nassif, A.Y.; Nguyen-Minh, L. Efficacy of CFRP/BFRP laminates in flexurally strengthening of concrete beams with corroded reinforcement. *J. Build. Eng.* **2022**, *53*, 104606. [CrossRef]
31. Li, J.; Xie, J.; Liu, F.; Lu, Z.A. Critical review and assessment for FRP concrete bond systems with epoxy resin exposed to chloride environments. *Compos. Struct.* **2019**, *229*, 111372. [CrossRef]
32. Abbood, I.S.; Odaa, S.A.; Hasan, K.F.; Jasim, M.A. Properties evaluation of fiber reinforced polymers and their constituent materials used in structures—A review. *Mater. Today Proc.* **2020**, *43*, 1003–1008. [CrossRef]
33. Berardi, U.; Dembsey, N. Thermal and fire characteristics of FRP composites for architectural applications. *Polymers* **2015**, *7*, 2276–2289. [CrossRef]
34. Sharifianjazi, F.; Zeydi, P.; Bazli, M.; Esmailkhanian, A.; Rahmani, R.; Bazli, L.; Khaksar, S. Fibre reinforced polymer reinforced concrete members under elevated temperatures: A review on structural performance. *Polymers* **2022**, *14*, 472. [CrossRef]
35. Tipirneni, R.R. Characterization of thermal and electrical properties of fiber reinforced polymer (FRP) composites. In *Graduate Theses, Dissertations, and Problem Reports*; West Virginia University: Morgantown, WV, USA, 2008. Available online: <https://researchrepository.wvu.edu/etd/1991> (accessed on 18 March 2023).
36. Liu, P.; Feng, R.; Wang, F.; Xu, Y.; Zhu, J.H. Fatigue testing of corroded RC continuous beams strengthened with polarized C-FRCM plate under ICCP-SS dual-function retrofitting system. *Structures* **2022**, *43*, 12–27. [CrossRef]
37. Elghazy, M.; Refai, E.A.; Ebead, U.; Nanni, A. Effect of corrosion damage on the flexural performance of RC beams strengthened with FRCM composites. *Compos. Struct.* **2017**, *180*, 994–1006. [CrossRef]
38. ACI 549.4R-13—Guide to Design and Construction of Externally Bonded Fabric-Reinforced Cementitious Matrix (FRCM) Systems for Repair and Strengthening Concrete and Masonry Structures; American Concrete Institute: Farmington Hills, MI, USA, 2013.
39. Ebead, U.; El-Sherif, H.E. Near surface embedded-FRCM for flexural strengthening of reinforced concrete beams. *Constr. Build. Mater.* **2019**, *204*, 166–176. [CrossRef]
40. Elghazy, M.; El Refai, A.; Ebead, U.; Nanni, A. Post repair flexural performance of corrosion-damaged beams rehabilitated with fabric-reinforced cementitious matrix (FRCM). *Constr. Build. Mater.* **2018**, *166*, 732–744. [CrossRef]
41. Elghazy, M.; El Refai, A.; Ebead, U.; Nanni, A. Fatigue and monotonic behaviors of corrosion-damaged reinforced concrete beams strengthened with FRCM composites. *J. Compos. Constr.* **2018**, *22*, 5. [CrossRef]
42. Hou, L.; Wang, J.; Huang, T.; Shen, C.; Aslani, F.; Chen, D. Flexural behaviour of corroded reinforced concrete beams repaired with ultra-high toughness cementitious composite. *Constr. Build. Mater.* **2019**, *211*, 1127–1137. [CrossRef]
43. Zheng, A.; Liu, Z.; Li, F.; Li, S. Experimental investigation of corrosion damaged RC beams strengthened in flexure with FRP grid-reinforced ECC matrix composites. *Eng. Struct.* **2021**, *244*, 112779. [CrossRef]
44. Jayasree, S.; Ganesan, N.; Abraham, R. Effect of ferrocement jacketing on the flexural behavior of beams with corroded reinforcements. *Constr. Build. Mater.* **2016**, *121*, 92–99. [CrossRef]
45. Kaish, A.B.M.A.; Jamil, M.; Raman, S.N.; Zain, M.F.M.; Nahar, L. Ferrocement composites for strengthening of concrete columns: A review. *Constr. Build. Mater.* **2018**, *160*, 326–340. [CrossRef]
46. Shannag, M.J.; Mourad, S.M. Flowable high strength cementitious matrices for ferrocement applications. *Constr. Build. Mater.* **2012**, *36*, 933–939. [CrossRef]
47. Chellapandian, M.; Prakash, S.S. Applications of fabric reinforced cementitious mortar (FRCM) in structural strengthening. *Compos. Sci. Tech.* **2021**, 201–233. [CrossRef]
48. Zheng, Y.; Wang, W.; Mosalam, K.M.; Fang, Q.; Chen, L. Experimental investigation and numerical analysis of RC beams shear reinforces with FRP/ECC composite layer. *Compos. Struct.* **2020**, *246*, 112436. [CrossRef]
49. Zheng, A.; Li, S.; Zhang, D.F.; Yan, Y. Shear strengthening of RC beams with corrosion damaged stirrups using FRP grid-reinforced ECC matrix composites. *Compos. Struct.* **2021**, *272*, 114229. [CrossRef]
50. Hu, B.; Zhou, Y.; Xing, F.; Sui, L.; Luo, M. Experimental and theoretical investigation on the hybrid CFRP-ECC flexural strengthening of RC beams with corroded longitudinal reinforcement. *Eng. Struct.* **2019**, *200*, 109717. [CrossRef]

51. Wu, C.; Li, V.C. CFRP-ECC hybrid for strengthening of the concrete structures. *Compos. Struct.* **2017**, *178*, 372–382. [[CrossRef](#)]
52. Maheswaran, J.; Chellapandian, M.; Subramanian, M.V.R.; Murali, G.; Vatin, N.I. Experimental and numerical investigation of shear behavior of engineered cementitious composite beams comprising fibers. *Materials* **2022**, *15*, 5059. [[CrossRef](#)]
53. George, M.; Sathyan, D.; Mini, K.M. Investigations on effect of different fibers on the properties of engineered cementitious composites. *Mater. Today Proc.* **2021**, *42*, 1417–1421. [[CrossRef](#)]
54. Akinyemi, B.A.; Omoniyi, T.E. Repair and strengthening of bamboo reinforced acrylic polymer modified square concrete columns using ferrocement jackets. *Sci. Afr.* **2020**, *8*, e00378. [[CrossRef](#)]
55. Boban, J.M.; John, S.A. A review on the use of ferrocement with stainless steel mesh as a rehabilitation technique. *Mater. Today Proc.* **2020**, *42*, 1100–1105. [[CrossRef](#)]
56. Aules, W.A.; Saeed, Y.M.; Al-Azzawi, H.; Rad, F.N. Experimental investigation on short concrete columns laterally strengthened with ferrocement and CFRP. *Case Stud. Constr. Mater.* **2022**, *16*, 2214–5095. [[CrossRef](#)]
57. Qiao, F.; Chau, C.K.; Li, Z. Property evaluation of magnesium phosphate cement mortar as patch repair material. *Constr. Build. Mater.* **2010**, *24*, 695–700. [[CrossRef](#)]
58. Ortega, I.; Pellicer, T.M.; Calderón, P.A.; Adam, J.M. Cement based mortar patch repair of RC columns. comparison with all-four-sides and one-side repair. *Constr. Build. Mater.* **2018**, *186*, 338–350. [[CrossRef](#)]
59. Ghoddousi, P.; Haghtalab, M.; Javid, A.A.S. Experimental and numerical analysis of the effects of different repair mortars on the controlling factors of macro-cell corrosion in concrete patch repair. *Cem. Concr. Compos.* **2021**, *121*, 104077. [[CrossRef](#)]
60. Pellegrino, C.; da Porto, F.; Modena, C. Rehabilitation of reinforced concrete axially loaded elements with polymer-modified cementitious mortar. *Constr. Build. Mater.* **2009**, *23*, 3129–3137. [[CrossRef](#)]
61. Da Porto, F.; Stievanin, E.; Pellegrino, C. Efficiency of RC square columns repaired with polymer-modified cementitious mortars. *Cem. Concr. Compos.* **2012**, *34*, 545–555. [[CrossRef](#)]
62. Zhang, C.; Guan, X.; Tian, J.; Li, Y.; Lyu, J. Corrosion resistance of RC/UHTCC beams with various healing promoters in marine environment. *Cement. Conc. Compos.* **2022**, *131*, 104604. [[CrossRef](#)]
63. Hou, L.; Zhou, B.; Guo, S.; Aslani, F.; Chen, D. Corrosion behavior and flexural performance of reinforced concrete/ultrahigh toughness cementitious composite (RC/UHTCC) beams under sustained loading and shrinkage cracking. *Constr. Build. Mater.* **2019**, *198*, 278–287. [[CrossRef](#)]
64. Loring, H.B.; Davids, W.G. Mechanically fastened hybrid composite strips for flexural strengthening of concrete beams. *Const. Build. Mater.* **2015**, *76*, 118–129. [[CrossRef](#)]
65. Hadhood, A.; Agamy, M.H.; Abdelsalam, M.M.; Mohamed, H.M.; El-Sayed, T.A. Shear strengthening of hybrid externally-bonded mechanically-fastened concrete beams using short CFRP strips: Experiments and theoretical evaluation. *Eng. Struct.* **2019**, *201*, 109795. [[CrossRef](#)]
66. Abuodeh, O.R.; Abdalla, J.A.; Hawileh, R.A. Flexural strengthening of RC beams using aluminum alloy plates with mechanically-fastened anchorage systems: An experimental investigation. *Eng. Struct.* **2021**, *234*, 109795. [[CrossRef](#)]
67. Feng, R.; Zhang, J.; Li, Y.; Zhu, J. Experimental study on hysteretic behavior for corroded circular RC columns retrofitted by ICCP-SS. *Structures* **2022**, *35*, 421–435. [[CrossRef](#)]
68. Su, M.; Zeng, C.; Li, W.; Zhu, J.H.; Lin, W.; Ueda, T.; Xing, F. Flexural performance of corroded continuous RC beams rehabilitated by ICCP-SS. *Compos. Struct.* **2020**, *232*, 111556. [[CrossRef](#)]
69. Su, M.; Wei, L.; Liang, H.; Zhu, J.H.; Ueda, T.; Xing, F. Fatigue behaviour and design of corroded reinforced concrete beams intervened by ICCP-SS. *Compos. Struct.* **2021**, *261*, 113295. [[CrossRef](#)]
70. Hu, J.; Wang, S.; Lu, Y.; Li, S. Investigation on efficiency of cathodic protection applied on steel in concrete cylinder with cfrp wrap serving as anode. *Case Stud. Constr. Mater.* **2022**, *17*, e01389. [[CrossRef](#)]
71. Hu, J.Y.; Zhang, S.S.; Chen, E.; Li, W.G. A review on corrosion detection and protection of existing reinforced concrete (RC) structures. *Constr. Build. Mater.* **2022**, *325*, 126718. [[CrossRef](#)]
72. Pourbaix, M. *Atlas of Electrochemical Equilibria in Aqueous Solutions*, 2nd ed.; National Association of Corrosion Engineers: Houston, TX, USA, 1974.
73. Ahmad, Z. *Basic Concepts in Corrosion in Principles of Corrosion Engineering and Corrosion Control*; Elsevier: Amsterdam, The Netherlands, 2006. [[CrossRef](#)]
74. Zhou, Y.; Gencturk, B.; Willam, K.; Attar, A. Carbonation-induced and chloride-induced corrosion in reinforced concrete structures. *J. Mater. Civil. Eng.* **2015**, *27*, 9. [[CrossRef](#)]
75. Liu, M. Finite element analysis of pitting corrosion on mechanical behavior of E690 steel panel. *Anti-Corros. Methods Mater.* **2022**, *69*, 4. [[CrossRef](#)]
76. Ghanem, H.; Trad, A.; Dandachy, M.; Elkordi, A. Effect of wet-mat curing time on chloride permeability of concrete bridge decks. In Proceedings of the International Congress and Exhibition, Sustainable Civil Infrastructures: Innovative Infrastructure Geotechnology, online, 28 October 2018; pp. 194–208. [[CrossRef](#)]
77. Rengaraju, S.; Pillai, R.G. An accelerated chloride threshold test for uncoated steel in highly resistive cementitious systems (Hr-ACT test). *Constr. Build. Mater.* **2021**, *305*, 124797. [[CrossRef](#)]
78. Verstryng, E.; Steen, C.V.; Vandecruys, E.; Wevers, M. Steel corrosion damage monitoring in reinforced concrete structures with the acoustic emission technique: A review. *Constr. Build. Mater.* **2022**, *349*, 128732. [[CrossRef](#)]

79. Angst, U.; Elsener, B.; Larsen, C.K.; Vennesland, O. Critical chloride content in reinforced concrete—A review. *Cem. Concr. Res.* **2009**, *39*, 1122–1138. [[CrossRef](#)]
80. De Vera, G.; Anton, C.; Lopez, M.P.; Climent, M.A. Depassivation time estimation in reinforced concrete structures exposed to chloride ingress: A probabilistic approach. *Cem. Concr. Compos.* **2017**, *79*, 21–33. [[CrossRef](#)]
81. Muthulingam, S.; Rao, B.N. Non-uniform time-to-corrosion initiation in steel reinforced concrete under chloride environment. *Corrosion Sci.* **2014**, *82*, 304–315. [[CrossRef](#)]
82. Poupard, O.; L'Hostis, V.; Catinaud, S.; Petre-Lazar, I. Corrosion damage diagnosis of a reinforced concrete beam after 40 years natural exposure in marine environment. *Cem. Concr. Res.* **2006**, *36*, 504–520. [[CrossRef](#)]
83. Jung, J.S.; Lee, B.Y.; Lee, K.S. Experimental study on the structural performance degradation of corrosion-damaged reinforced concrete beams. *Adv. Civil Eng.* **2019**, *2019*, 9562574. [[CrossRef](#)]
84. Kharma, K.M.; Ahmad, S.; Al-Osta, M.A.; Maslehuddin, M.; Al-Huri, M.; Khalid, H.; Al-Dulaijan, S.U. Experimental and analytical study on the effect of different repairing and strengthening strategies on flexural performance of corroded RC beams. *Structures* **2022**, *46*, 336–352. [[CrossRef](#)]
85. Masoud, S.; Soudki, K.; Topper, T. CFRP-strengthened and corroded RC beams under monotonic and fatigue loads. *J. Compos. Constr. ASCE* **2001**, *5*, 228. [[CrossRef](#)]
86. Liu, M. Effect of uniform corrosion on mechanical behavior of E690 high strength steel lattice corrugated panel in marine environment: A finite element analysis. *Mater. Res. Express.* **2021**, *8*, 066510. [[CrossRef](#)]
87. Nossoni, G.; Harichandran, R.S.; Baiyasi, M.I. Rate of reinforcement corrosion and stress concentration in concrete columns repaired with bonded and unbonded FRP wraps. *J. Compos. Constr.* **2015**, *19*, 04014080. [[CrossRef](#)]
88. Zheng, Y.; Zheng, S.S.; Yang, L.; Dong, L.G.; Ruan, S.; Ming, M. Experimental study on the seismic behavior of corroded reinforced concrete walls in an artificial climate corrosion environment. *Eng. Struct.* **2022**, *252*, 113469. [[CrossRef](#)]
89. Zheng, Y.; Zheng, S.S.; Yang, L.; Dong, L.G.; Ruan, S. Experimental study and numerical model of the seismic behavior of reinforced concrete beams in an artificial corrosion environment. *J. Build. Eng.* **2022**, *46*, 103705. [[CrossRef](#)]
90. Saraswathy, V.; Lee, H.S.; Karthick, S.; Kwon, S.J. Extraction of chloride from chloride contaminated concrete through electrochemical method using different anodes. *Constr. Build. Mater.* **2018**, *158*, 549–562. [[CrossRef](#)]
91. Fajardo, G.; Escadeillas, G.; Arliguie, G. Electrochemical chloride extraction (ECE) from steel-reinforced concrete specimens contaminated by artificial sea-water. *Corros. Sci.* **2006**, *48*, 110–125. [[CrossRef](#)]
92. Zhu, J.H.; Wei, L.; Wang, Z.; Liang, C.K.; Fang, Y.; Xing, F. Application of carbon-fiber-reinforced polymer anode in electrochemical chloride extraction of steel-reinforced concrete. *Constr. Build. Mater.* **2016**, *120*, 275–283. [[CrossRef](#)]
93. Souza, L.R.D.A.; Medeiros, M.H.F.D.; Pereira, E.; Capraro, A.P.B. Electrochemical chloride extraction: Efficiency and impact on concrete containing 1% of NaCl. *Constr. Build. Mater.* **2017**, *145*, 435–444. [[CrossRef](#)]
94. Hu, J.; Li, S.; Lu, Y.; Zhang, H.; Zhang, M. Efficiency of electrochemical extraction of chlorides in fly ash concrete using carbon fibre mesh anode. *Constr. Build. Mater.* **2020**, *249*, 118717. [[CrossRef](#)]
95. Jin, Z.; Hou, D.; Zhao, T. Electrochemical chloride extraction (ECE) based on the high performance conductive cement-based composite anode. *Constr. Build. Mater.* **2018**, *173*, 149–159. [[CrossRef](#)]
96. Do-Dai, K.; Liu, C.; Lu, D.G.; Yu, X.H. Experimental investigation on seismic behavior of corroded RC columns under artificial climate environment and electrochemical chloride extraction: A comparative study. *Constr. Build. Mater.* **2020**, *242*, 118014. [[CrossRef](#)]
97. Zhu, W.; Francois, R.; Liu, Y. Propagation of corrosion and corrosion patterns of bars embedded in reinforced concrete beams stored in chloride environment for various periods. *Constr. Build. Mater.* **2017**, *145*, 147–156. [[CrossRef](#)]
98. Liu, M.; Cheng, X.; Li, X.; Hu, J.; Pan, Y.; Jin, Z. Indoor accelerated corrosion test and marine field test of corrosion-resistant low-alloy steel rebars. *Case Stud. Constr. Mater.* **2016**, *5*, 87–99. [[CrossRef](#)]
99. Qian, S.; Zhang, J.; Qu, D. Theoretical and experimental study of microcell and macrocell corrosion in patch repairs of concrete structures. *Cem. Concr. Compos.* **2006**, *28*, 685–695. [[CrossRef](#)]
100. Fakhri, H.; Ragalwar, K.A.; Ranade, R. On the use of strain-hardening cementitious composite covers to mitigate corrosion in reinforced concrete structures. *Constr. Build. Mater.* **2019**, *224*, 850–862. [[CrossRef](#)]
101. Li, Q.; Jin, X.; Yan, D.; Fu, C.; Xu, J. Study of wiring method on accelerated corrosion of steel bars in concrete. *Constr. Build. Mater.* **2021**, *269*, 121286. [[CrossRef](#)]
102. Wang, Y.; Cao, Y.; Zhang, P. Water absorption and chloride diffusivity of concrete under the coupling effect of uniaxial compressive load and freeze-thaw cycles. *Constr. Build. Mater.* **2019**, *209*, 566–576. [[CrossRef](#)]
103. Wang, Z.; Zeng, Q.; Wang, L.; Yao, Y.; Li, K. Corrosion of rebar in concrete under cyclic freeze-thaw and Chloride salt action. *Constr. Build. Mater.* **2014**, *53*, 40–47. [[CrossRef](#)]
104. Cheng, Y.; Zhang, Y.; Jiao, Y.; Yang, J. Quantitative analysis of concrete property under effects of crack, freeze-thaw and carbonation. *Constr. Build. Mater.* **2016**, *129*, 106–115. [[CrossRef](#)]
105. Yao, X.; Zhang, M.; Guan, J.; Li, L.; Bai, W.; Liu, Z. Research on the corrosion damage mechanism of concrete in two freeze-thaw environments. *Adv. Civil Eng.* **2020**, *2020*, 8839386. [[CrossRef](#)]
106. Liu, K.; Yan, J.; Meng, X.; Zou, C. Bond behavior between deformed steel bars and recycled aggregate concrete after freeze-thaw cycles. *Constr. Build. Mater.* **2020**, *232*, 117236. [[CrossRef](#)]

107. Lu, X.C.; Guan, B.; Chen, B.F.; Zhang, X.; Xiong, B.B. The effect of freeze-thaw damage on corrosion in reinforced concrete. *Adv. Mater. Sci. Eng.* **2021**, *2021*, 9924869. [\[CrossRef\]](#)
108. Shang, Z.; Zheng, S.; Zheng, H.; Li, Y.L.; Dong, J. Seismic behavior and damage evolution of corroded RC columns designed for bending failure in an artificial climate. *Structures* **2022**, *38*, 184–201. [\[CrossRef\]](#)
109. ASTM-G102–89; Standard Practice for Calculation of Corrosion Rates and Related Information from Electrochemical Measurements. ASTM: West Conshohocken, PA, USA, 2015.
110. Joshi, J.; Arora, H.C.; Sharma, U.K. Structural performance of differently confined and strengthened corroding reinforced concrete columns. *Constr. Build. Mater.* **2015**, *82*, 287–295. [\[CrossRef\]](#)
111. Jia, J.; Zhao, L.; Wu, S.; Wang, X.; Bai, Y.; Wei, Y. Experimental investigation on the seismic performance of low-level corroded and retrofitted reinforced concrete bridge columns with CFRP fabric. *Eng. Struct.* **2020**, *209*, 110225. [\[CrossRef\]](#)
112. Siad, A.; Bencheikh, M.; Hussein, L. Effect of combined pre-cracking and corrosion on the method of repair of concrete beams. *Constr. Build. Mater.* **2017**, *132*, 462–469. [\[CrossRef\]](#)
113. Zhang, H.; Wu, J.; Jin, F.; Zhang, C. Effect of corroded stirrups on shear behavior of reinforced recycled aggregate concrete beams strengthened with carbon fiber-reinforced polymer. *Compos. B Eng.* **2019**, *161*, 357–368. [\[CrossRef\]](#)
114. Daneshvar, K.; Moradi, M.J.; Ahmadi, K.; Hajiloo, H. Strengthening of corroded reinforced concrete slabs under multi-impact loading: Experimental results and numerical analysis. *Constr. Build. Mater.* **2021**, *284*, 122650. [\[CrossRef\]](#)
115. Alwash, N.; Kadhum, M.; Mahdi, A.M. Rehabilitation of corrosion-defected RC beam-column members using patch repair technique. *Buildings* **2019**, *9*, 120. [\[CrossRef\]](#)
116. Yuan, W.; Wang, X.; Dong, Z.; Zhou, P.; Wang, Q. Cyclic loading test for RC bridge piers strengthened with UHPC jackets in the corrosive environment. *Soil Dyn. Earthq. Eng.* **2022**, *158*, 107290. [\[CrossRef\]](#)
117. Rajput, A.S.; Sharma, U.K.; Engineer, K. Seismic retrofitting of corroded RC columns using advanced composite materials. *Eng. Struct.* **2019**, *181*, 35–46. [\[CrossRef\]](#)
118. Pantazopoulou, S.J.; Bonacci, J.F.; Sheikh, S.; Thomas, A.; Hearn, N. Repair of corrosion-damaged columns with FRP wraps. *J. Compos. Constr.* **2001**, *5*, 3–11. [\[CrossRef\]](#)
119. Shen, D.; Yang, Q.; Huang, C.; Cui, Z.; Zhang, J. Tests on seismic performance of corroded reinforced concrete shear walls repaired with basalt fiber-reinforced polymers. *Constr. Build. Mater.* **2019**, *209*, 508–521. [\[CrossRef\]](#)
120. Wang, C.Y.; Shih, C.C.; Hong, S.C.; Hwang, W.C. Rehabilitation of cracked and corroded reinforced concrete beams with fiber-reinforced plastic patches. *J. Compos. Constr.* **2004**, *8*, 219–228. [\[CrossRef\]](#)
121. Li, M.; Shen, D.; Yang, Q.; Cao, X.; Liu, C.; Kang, J. Rehabilitation of seismic-damaged reinforced concrete beam-column joints with different corrosion rates using basalt fiber-reinforced polymer sheets. *Compos. Struct.* **2022**, *289*, 115397. [\[CrossRef\]](#)
122. Yousefi, O.; Narmashiri, K.; Hedayat, A.A.; Karbakhsh, A. Strengthening of corroded steel CHS columns under axial compressive loads using CFRP. *J. Constr. Steel Res.* **2021**, *178*, 106496. [\[CrossRef\]](#)
123. Tastani, S.P.; Pantazopoulou, S.J. Experimental evaluation of FRP jackets in upgrading RC corroded columns with substandard detailing. *Eng. Struct.* **2004**, *26*, 817–829. [\[CrossRef\]](#)
124. Triantafyllou, G.G.; Rousakis, T.C.; Karabinis, A.I. Corroded RC beams patch repaired and strengthened in flexure with fiber-reinforced polymer laminates. *Compos. B Eng.* **2017**, *112*, 125–136. [\[CrossRef\]](#)
125. Ray, I.; Parish, G.C.; Davalos, J.F.; Chen, A. Effect of concrete substrate repair methods for beams aged by accelerated corrosion and strengthened with CFRP. *J. Aerosp. Eng.* **2011**, *24*, 227–239. [\[CrossRef\]](#)
126. Lee, C.; Bonacci, J.F.; Thomas, M.D.; Maalej, M.; Khajepour, S.; Hearn, N.; Pantazopoulou, S.; Sheikh, S. Accelerated corrosion and repair of reinforced concrete columns using carbon fibre reinforced polymer sheets. *Can. J. Civil. Eng.* **2000**, *27*, 941–948. [\[CrossRef\]](#)
127. El Maaddawy, T.; Soudki, K. Carbon-fiber-reinforced polymer repair to extend service life of corroded reinforced concrete beams. *J. Compos. Constr.* **2005**, *9*, 187–194. [\[CrossRef\]](#)
128. Sahmaran, M.; Li, V.; Andrade, C. Corrosion resistance performance of steel-reinforced engineered cementitious composite beams. *ACI Mater. J.* **2008**, *105*, 243–250. [\[CrossRef\]](#)
129. El-Maaddawy, T.A. Mechanically fastened composites for retrofitting corrosion-damaged reinforced-concrete beams: Experimental investigation. *J. Compos. Constr.* **2014**, *18*, 04013041. [\[CrossRef\]](#)
130. Radhi, M.S.; Hassan, M.S.; Gorgis, I.N. Carbon fibre-reinforced polymer confinement of corroded circular concrete columns. *J. Build. Eng.* **2021**, *43*, 102611. [\[CrossRef\]](#)
131. Al-Akhras, N.; Al-Mashraqi, M. Repair of corroded self-compacted reinforced concrete columns loaded eccentrically using carbon fiber reinforced polymer. *Case Stud. Constr. Mater.* **2021**, *14*, e00476. [\[CrossRef\]](#)
132. Liu, X.; Li, Y. Experimental study of seismic behavior of partially corrosion-damaged reinforced concrete columns strengthened with FRP composites with large deformability. *Constr. Build. Mater.* **2018**, *191*, 1071–1081. [\[CrossRef\]](#)
133. Li, W.; Huang, Z.; Huang, Z.; Yang, X.; Shi, T.; Xing, F. Shear Behavior of RC Beams with Corroded Stirrups Strengthened Using FRP Laminates: Effect of the Shear Span-to-Depth Ratio. *J. Compos. Constr.* **2020**, *24*, 0001042. [\[CrossRef\]](#)
134. Kreit, A.; Al-Mahmoud, F.; Castel, A.; Francois, R. Repairing corroded RC beam with near-surface mounted CFRP rods. *Mater. Struct.* **2011**, *44*, 1205–1217. [\[CrossRef\]](#)
135. Al-Hammoud, R.; Soudki, K.; Topper, T.H. Fatigue flexural behavior of corroded reinforced concrete beams repaired with CFRP sheets. *J. Compos. Constr.* **2011**, *15*, 42–51. [\[CrossRef\]](#)

136. Xie, J.H.; Hu, R.L. Experimental study on rehabilitation of corrosion-damaged reinforced concrete beams with carbon fiber reinforced polymer. *Constr. Build. Mater.* **2013**, *38*, 708–716. [[CrossRef](#)]
137. Al-Majidi, M.H.; Lampropoulos, A.P.; Cundy, A.B.; Tsioulou, O.T.; Alrekabi, S. Flexural performance of reinforced concrete beams strengthened with fibre reinforced geopolymer concrete under accelerated corrosion. *Structures* **2019**, *19*, 394–410. [[CrossRef](#)]
138. Fang, S.; Lam, E.S.S.; Wong, W.Y. Using alkali-activated slag ferrocement to strengthen corroded reinforced concrete columns. *Mater. Struct.* **2017**, *50*, 35. [[CrossRef](#)]
139. Elghazy, M.; El Refai, A.; Usama, E.; Nanni, A. Corrosion-damaged RC beams repaired with fabric-reinforced cementitious matrix. *J. Compos. Constr.* **2018**, *22*, 04018039. [[CrossRef](#)]
140. Hou, L.; Guo, S.; Zhou, B.; Chen, D.; Aslani, F. Bond-slip behaviour of corroded reinforcement and ultra-high toughness cementitious composite in flexural members. *Constr. Build. Mater.* **2019**, *196*, 185–194. [[CrossRef](#)]
141. Zhu, J.; Su, M.; Huang, J.; Ueda, T.; Xing, F. The ICCP-SS technique for retrofitting reinforced concrete compressive members subjected to corrosion. *Constr. Build. Mater.* **2018**, *167*, 669–679. [[CrossRef](#)]
142. Raju, P.M. Retrofitting of reinforced concrete structural elements-Recent technologies and future scope. *Int. J. Sci. Res. Eng. Technol. (IJSRSET)* **2017**, *3*, 47–60.
143. Hussain, M.; Sharif, A.; Basunbul, I.A.; Baluch, M.H.; Al-sulaimani, G.J. Flexural behavior of precracked reinforced concrete beams strengthened externally by steel plates. *ACI Struct. J.* **1995**, *92*, 14–23.
144. Zhang, X.; Wu, Z.; Cheng, Y. An approach of steel plate hybrid bonding technique to externally bonded fibre-reinforced polymer strengthening system. *Int. J. Distrib. Sens.* **2018**, *14*, 1550147718786455. [[CrossRef](#)]
145. Jones, R.; Swamy, R.N.; Charif, A. Plate separation and anchorage of reinforced concrete beams strengthened by epoxy-bonded steel plates. *Struct. Eng.* **1988**, *66*, 85–94.
146. Salah, A.; Elsanadedy, H.; Abbas, H.; Almusallam, T.; Al-Salloum, Y. Behavior of axially loaded I-shaped RC columns strengthened using steel jacketing. *J. Build. Eng.* **2022**, *47*, 103870. [[CrossRef](#)]
147. Sudha, C.; Sambasivan, A.K.; Rajkumar, P.R.K.; Sudha, C.J.M.; Sambasivan, A.K.; Rajkumar, P.R.K.; Jegan, M. Investigation on the performance of reinforced concrete columns jacketed by conventional concrete and geopolymer concrete. *Eng. Sci. Tech.* **2022**, *36*, 101275. [[CrossRef](#)]
148. Maheswaran, J.; Chellapandian, M.; Arunachalam, N. Retrofitting of severely damaged RC members using fiber reinforced polymer composites: A comprehensive review. *Structures* **2022**, *38*, 1257–1276. [[CrossRef](#)]
149. Chellapandian, M.; Prakash, S.S. Behavior of FRP strengthened reinforced concrete columns under pure compression—Experimental and numerical studies. In *Recent Advances in Structural Engineering: Select Proceedings of SEC*; Springer: Singapore, 2016; Volume 2, pp. 663–673.
150. Jain, S.; Chellapandian, M.; Prakash, S.S. Emergency repair of severely damaged reinforced concrete column elements under axial compression: An experimental study. *Constr. Build. Mater.* **2017**, *155*, 751–761. [[CrossRef](#)]
151. Chellapandian, M.; Prakash, S.S. Rapid repair of severely damaged reinforced concrete columns under combined axial compression and flexure: An experimental study. *Constr. Build. Mater.* **2018**, *173*, 368–380. [[CrossRef](#)]
152. *ACI 440.2R-17*; Guide for the Design and Construction of Externally Bonded FRP System for Strengthening Concrete Structures. ACI Committee 440; American Concrete Institute: Farmington Hills, MI, USA, 2017; p. 45.
153. Kuntal, V.S.; Chellapandian, M.; Prakash, S.S.; Sharma, A. Experimental study on the effectiveness of inorganic bonding Materials for NSM shear strengthening of prestressed concrete beams. *Fibers* **2020**, *8*, 40. [[CrossRef](#)]
154. Kuntal, V.S.; Chellapandian, M.; Prakash, S.S. Efficient near surface mounted CFRP shear strengthening of high strength prestressed concrete beams—An experimental study. *Compos. Struct.* **2017**, *180*, 16–28. [[CrossRef](#)]
155. Chellapandian, M.; Prakash, S.S.; Sharma, A. Strength and ductility of innovative hybrid NSM reinforced and FRP confined short RC columns under axial compression. *Compos. Struct.* **2017**, *176*, 205–216. [[CrossRef](#)]
156. Kuntal, V.S.; Chellapandian, M.; Prakash, S.S. Effect of geopolymer based mortar as a bonding material on NSM CFRP shear strengthening of high strength prestressed concrete beams. In *Proceedings of the ICCMS 2017*, Hyderabad, India, 27–29 December 2017.
157. Chinthapalli, H.K.; Chellapandian, M.; Agarwal, A.; Prakash, S.S. Effectiveness of hybrid fibre-reinforced polymer retrofitting on behaviour of fire damaged RC columns under axial compression. *Eng. Struct.* **2020**, *211*, 110458. [[CrossRef](#)]
158. Chellapandian, M.; Jain, S.; Prakash, S.S.; Sharma, A. Effect of cyclic damage on the performance of RC square columns strengthened using hybrid FRP composites under Axial Compression. *Fibers* **2019**, *7*, 90. [[CrossRef](#)]
159. Chellapandian, M.; Prakash, S.S.; Rajagopal, A. Analytical and FE studies on hybrid FRP strengthened RC square column elements under axial and eccentric compression. *Compos. Struct.* **2018**, *184*, 234–248. [[CrossRef](#)]
160. Chellapandian, M.; Jain, S.; Prakash, S.S. Rapid repair of pre-damaged RC square columns using hybrid FRP strengthening under axial compression. In *Proceedings of the 3rd R.N. Raikar Memorial International Conference: Gettu-Kodur International Symposium*, ACI India Chapter, Mumbai, India, 14–15 December 2018; Volume 1, pp. 431–436.
161. Chellapandian, M.; Prakash, S.S. Axial compression–Bending interaction behavior of severely damaged RC columns repaired using Hybrid FRP composites. *Struct. Eng. Conv.* **2018**, *195*, 390–404. [[CrossRef](#)]
162. Chellapandian, M.; Prakash, S.S. Behavior of hybrid NSM reinforced and externally confined short RC columns under eccentric compression—Experimental and numerical studies. In *Proceedings of the 71st RILEM Annual Week & ICACMS 2017*, Chennai, India, 3–8 September 2017; pp. 519–528.

163. Siddika, A.; Mamun, M.A.A.; Alyousef, R.; Amran, Y.H.M. Strengthening of reinforced concrete beams by using fiber reinforced polymer composites: A review. *Build. Eng.* **2019**, *25*, 100798. [[CrossRef](#)]
164. Li, J.; Gong, J.; Wang, L. Seismic behavior of corrosion-damaged reinforced concrete columns strengthened using combined carbon fiber-reinforced polymer and steel jacket. *Constr. Build. Mater.* **2009**, *23*, 2653–2663. [[CrossRef](#)]
165. Waghmare, D.; Chellapandian, M.; Prakash, S.S. Analytical studies on the pure compression behavior of pre-damaged RC columns strengthened using hybrid FRP composites. In Proceedings of the International Conference on ICCRS, Mumbai, India, 30 November–1 December 2019.
166. Elghazy, M.; El Refai, A.; Ebead, U.; Nanni, A. Experimental results and modelling of corrosion-damaged concrete beams strengthened with externally-bonded composites. *Eng. Struct.* **2018**, *172*, 172–186. [[CrossRef](#)]
167. Zhang, F.; Zhang, W.; Hu, Z.; Jin, L.; Jia, X.; Wu, L.; Wan, Y. Experimental and numerical analysis of the mechanical behaviors of large scale composite c-beams fastened with multi-bolt joints under four-point bending load. *Compos. B Eng.* **2019**, *164*, 168–178. [[CrossRef](#)]
168. Ghanem, H.; Phelan, S.; Senadheera, S.; Pruski, K. Chloride ion transport in bridge deck concrete under different curing durations. *J. Bridge Eng.* **2008**, *13*, 218. [[CrossRef](#)]

Disclaimer/Publisher’s Note: The statements, opinions and data contained in all publications are solely those of the individual author(s) and contributor(s) and not of MDPI and/or the editor(s). MDPI and/or the editor(s) disclaim responsibility for any injury to people or property resulting from any ideas, methods, instructions or products referred to in the content.